University of Stavanger

FACULTY OF SCIENCE AND TECHNOLOGY

MASTER'S THESIS

Study programme/specialisation: Petroleum Engineering Master Reservoir Specialization	Spring semester, 2018 Open
Author: Eliana Pulido Vasquez	…… (signature of author)

Supervisor(s): Pål Østebø Andersen, Dag Chun Standnes.

Title of master's thesis:

Relative Permeability and Capillary Pressure Estimation from Core-flooding Experiments studying Capillary End Effects

Credits:

30 ECTS

Keywords: Capillary End Effects Capillary Pressure Relative Permeability Experimental Design Core-flooding Laboratory Experiments	Number of pages: 74 + supplemental material/other: NA Stavanger, 16th July / 2018

Relative Permeability and Capillary Pressure Estimation from Core-flooding Experiments studying Capillary End Effects

By

Eliana Pulido Vásquez

Master Thesis

Presented to the Faculty of Energy Resources

University of Stavanger

University of Stavanger

July 2018

Acknowledgments

I would like to express my special thanks of gratitude to Andrés, Citra and Kenny for their time to discussion and their support during the extensive times in the lab.

My deepest appreciation goes to the Faculty supervisors Pål Østebø Andersen and Dag Chun Standnes for their exceptional guidance and academic support.

I would like to say "Thank you" to Reza, Ola and Kim, for their support in the lab and being willing to help when issues in the lab came along.

Many thanks to professor Aly for providing core material to conduct the flooding experiments.

Abstract

Relative Permeability and Capillary Pressure Estimation from Core-flooding Experiments studying Capillary End Effects

Relative permeability (Relperm) and capillary pressure (Cp) are fundamental input parameters to describe multiphase flow in a reservoir. Calculation of permeability and capillary pressure may be affected by Capillary End Effects (CEE) as a result of a significant change of capillary properties at the outflow face of the core. The outlet is characterized by zero capillary pressure. It induces the wetting phase to be trapped near the end of the core, leading to incorrect estimation of parameters such as saturation distribution and pressure drop. In this experiment, the core plugs were artificially treated to alter their wettability into more oil-wet conditions. It sought the oil phase to be trapped at the outlet end and then be recovered by step-wise increasing rates.

A procedure for measuring RelPerm and Capillary Pressure over the whole saturation range was used to study CEE. Capillary pressure data were collected from spontaneous and forced imbibition laboratory experiments, and Relperm curves were estimated by history matching of experimental oil production and pressure drop by using the simulator Sendra. End effects were seen when relying on a deliberate procedure that involves low flow rates, long periods of injection, and unsteady state method. Such End Effects were observed through gradual increments of oil production after a change in rate, especially at low rates. Vanished CEE were perceived when using higher rates even though those effects were not completely removed. These observations allow to conclude that waterflooding under unsteady state method is a rate-depend process when accounting for capillary end effects.

Contents

List of Figures

List of Tables

Nomenclature

A	Core cross sectional area (cm^2)
C_o	Corey oil exponent (dimensionless)
C_w	Corey water exponent (dimensionless)
dP	Differential Pressure (mbar)
i	Oil phase (o), or water phase (w)
K	Absolute Permeability (D)
k_o	Effective oil permeability (D)
k_{ro}	Oil relative permeability (D)
$k_{ro\ (max)}$	Oil relative permeability at maximum water saturation (D)
$k_{ro\ (Sor)}$	Oil Relative Permeability at Initial oil saturation (dimensionless)
$k_{ro\ (Swi)}$	Oil Relative Permeability at Initial water saturation (dimensionless)
k_{rw}	Water relative permeability (D)
$k_{rw\ (max)}$	Water relative permeability at maximum water saturation (D)
$k_{rw\ (Sor)}$	Water Relative Permeability at Initial oil saturation (dimensionless)
$k_{rw\ (Sorw)}$	Water relative permeability at residual oil (D)
$k_{rw\ (Swi)}$	Water Relative Permeability at Initial water saturation (dimensionless)
L	Length (cm)
M	Molarity (mol/l)
$m_{(Sat)}$	mass (g)
$m_{(Swi)}$	mass at initial water saturation (g)
Pc	Capillary pressure (mbar)
P_i	Inlet Pressure (mbar)
P_o	Outlet pressure (mbar)
P_{to}	Threshold Pressure of oil (mbar)
P_{tw}	Threshold Pressure of water (mbar)
Q	Flow rate (ml/s)
RelPerm	Relative Permeability (fraction)
S_o	Oil saturation (fraction)
S_{or}	Residual Oil saturation (fraction)
S_{or}	Residual Oil saturation after waterflooding (fraction)
S_w	Water saturation (fraction)
S_{wi}	(Irreducible) Initial Water saturation (fraction)
S_{wmax}	Maximum water saturation (fraction)
S_{wr}	Irreducible water saturation (fraction)
S_{wor}	Residual oil saturation after waterflooding (fraction)
V	Volume (ml)
λ	Mobility (fraction)
μ	Viscosity (cP)
ρ	Density (g/ml)
σ	Surface tension (dyn/cm)
φ	Porosity (%)

Abbreviations

CEE	Capillary End Effects
Cp	Centipoise
D	Darcy
EOR	Enhanced Oil Recovery
IFT	Interfacial Tension
PV	Pore Volume
SCAL	Special Core Analysis
MWB_1	First Mixed-wet Bentheimer
MWB_2	Second Mixed-wet Bentheimer
OWB_3	Oil-wet Bentheimer
OWBEREA	Oil-wet Berea

1. Introduction

Relative permeability (RelPerm) and capillary pressure (Pc) are fundamental input parameters to describe multiphase flow in reservoir engineering. These parameters are important for production forecasting, reserves estimates, and ultimate-recovery predictions. (Richardson et al., 1952; Civan and Donaldson, 1989). RelPerm data are usually obtained from steady and unsteady displacement experiments in the laboratory (Osoba et al., 1951; Heaviside and Black, 1983; Qadeer et al., 1988; Mohanty and Miller, 1991). For an unsteady-state test, one fluid, which is immiscible with the fluid in the core, is injected through the core to displace the fluid inside. On the other hand, in a steady-state test both immiscible fluids are injected co-currently at a specific ratio through the core until the same production ratios are achieved at the outlet (Civan and Donaldson, 1987).

Interpretation of data resulting from steady-state experiments is relatively simple, but it is difficult to obtain a constant average saturation of the fluids, and a long time is required to establish the saturation after each change. The unsteady-state method can be carried out in a relatively short time, and it tends to undergo Capillary End Effects (CEE) at the entrance and exit of the core, especially when low rates are used (Heaviside and Black, 1983; Qadeer et al., 1988; Honarpour and Mahmood, 1988)**.** Such effect is experienced when fluids pass from a region of finite capillary pressure in the sample to a region of zero capillary pressure in the end piece and tubing (Hinkley and Davis, 1986)**.** This discontinuity induces an accumulation of the phase (i.e. wetting or non-wetting phase where the saturation corresponds to zero at the end of the core), affecting transient production, saturation distribution, and pressure drop (Geffen et al., 1951; Richardson et al., 1952; Gupta and Maloney, 2016; Hadley and Handy, 1956; Osoba et al., 1951).

Numerous correlations between theoretical and experimental results are demonstrated in previous studies for the capillary effect. Virnovsky et al. (1995) proposed a steady-state technique that eliminates errors caused by Capillary End Effects in an attempt to find consistent values of saturation and phase relative permeability. Gupta and Maloney (2016) used their intercept model to correct pressure drops and saturation measurements during a steady state core-flooding test. Corrected data were subsequently used for calculating relative

permeability through Darcy's law. Qadeer et al. (1988) made corrections of relative permeability for CEE by means of in-situ saturation and independent measurements of capillary pressure vs saturation functions. They quantified changes in relative permeability with rate by combining their results from a series of capillary pressure experiments and a history matching software. Huang and Honarpour (1998) suggested corrections for both residual saturation and endpoint permeability affected by CEE. Based on these correlations, saturation curves were consistently predicted with experimental measurements. Hadley and Handy (1956) proposed a numerical formulation for steady state saturation profile and pressure drop resulting from the end effect. They introduced two dimensionless numbers which characterize the system and determine the magnitude of end effect. Kite and Rapoport (1958) provided a theory for waterflooding behavior in water-wet cores in presence of End Effects.

The present study conducts a series of flooding tests that intentionally induce CEE for the calculation of both Pc and RelPerm under unsteady state. The main objective of the research is to quantify RelPerm and Pc in a set-up with the influence of CEE by conducting: (1) A spontaneous imbibition test to measure the oil that is recovered by action of capillary forces; and (2) a forced imbibition test designed to recover the oil that remains trapped in the porous medium by the increment of advective forces (i.e. flow rates); they will be increased gradually to vary the dominance of capillary and advective forces. Tests are carried out on both a mixed-wet and oil-wet Bentheimer cores, whose wetting state has been altered by using Quilon L, a wettability altering agent. It must be highlighted that despite of using an unsteady state method, steady conditions in both pressure drop and oil production are targeted while injecting fluids at very low rates. In order to fulfil the primary objective, this research synthetizes an extensive volume of data from both spontaneous and forced imbibition tests. Likewise, it stablishes a procedure for obtaining RelPerm and Pc curves over the whole saturation range, taking on challenges like implementing very low injection rates, low-pressure drops, and lengthy periods when targeting stabilized trends.

Finally, oil production and pressure drop experimental data at steady conditions are input in a simulator for core analysis software, namely Sendra, to compute RelPerm and Capillary Pressure. Both parameters will be determined by simultaneous history matching of the experimental data.

2. Fundamental Theory

This section presents the basic definitions and theory that will support analysis and results for the present study. It will be focused towards Capillary Pressure and Relative Permeability principles and the implications of wetting condition on multiphase flow.

2.1. Wettability

Wettability describes the preference of a solid to be in contact with a fluid. Generally, the wettability of a porous system can be divided into two basic types: uniform and non-uniform. A porous system with uniform wettability namely i.e., strongly water-wet, strongly oil-wet or mixed-wet. Conversely, non-uniform or fractional wettability is characterized since the wettability paths are not connected as a result of rock mineral composition and oil contact Hwang et al. (2006).

In a water-wet system, the water will displace the oil from the rock surface, indicating that the rock surface "prefers" to be in contact with water rather than oil. Similarly, if an oil-wet core is saturated with water oil will imbibe into the core and displace water from the rock surface (Anderson, 1986). Depending on the specific interactions of rock, oil, and brine, the wettability of a system can range from strongly water-wet to strongly oil-wet. When the rock has no strong preference for either oil or water, the system is said to be of neutral (or mixed) wettability (Anderson, 1986). The term mixed-wettability was postulated by Salathiel (1973) to describe special form of heterogeneous wettability condition.

Besides strong and neutral wettability, fractional wettability is characteristic when different regions of the system have different wetting preferences (Brown and Fatt, 1956). It is important to distinguish fractional from intermediate wettability which is the lack of a strong wetting preference, meanwhile mixed-wetting which implicates a variety of preferences, possibly including intermediate-wetting conditions (Abdallah et al., 2007).

2.2. Single Phase Permeability

Permeability is the property of a porous medium that characterizes the ease which fluids flow through the porous medium in response to the applied fluid pressure gradient. However, permeability is not measured directly, but calculated from other physical measurements with various theoretical and empirical relationships. The relationship used in the hydrocarbon industry is the empirically derived in Darcy's Law in 1856 as described in **Equation (1)**. Glover, 2001.

Permeability is measured on cores in the laboratory by flowing a fluid of known viscosity through a core sample of known dimensions at a set rate, and measuring the pressure drop across the core, or by setting the fluid to flow at a set pressure difference and measuring the flow rate produced (Glover, 2000). Darcy's law can be described by:

$$u_i = -K\lambda_i \frac{\partial P_i}{\partial x} \quad (1)$$

Where:

i = oil phase (o), or water phase (w)

u_i = Flow rate (ml/s)

K = Absolute permeability of the porous medium (Darcy)

$\frac{\partial P_i}{\partial x}$ = Derivative of pressure as a function of distance (atm)

λ_i = Mobility

Darcy's law, is then, a proportional relationship between the instantaneous discharge rate through a porous medium, the viscosity of the fluid and the pressure drop over a given distance.

2.3. Relative Permeability and multiphase flow

Before entering upon the subject, it is remarkable to point out basic definitions for permeability. In a core sample, the *absolute permeability* (K) is a measure of the capacity of the core to transmit fluids thus, it is a property of the porous medium itself (Ahmed, 2001). If there are two fluids present in the core, the permeabilities of each fluid depend upon the

saturation of each fluid. These are called *effective permeabilities*, (i.e. k_w, k_o) which are function of the fluid saturation and the wetting characteristics of the sample (Glover, 2000). On the other hand, relative permeability is a direct measure of the ability of the porous system to conduct one fluid when one or more fluids are present. Then, the *relative permeability* **(Equation 2)** of each phase (oil and water) at a specific saturation is the ratio of the effective permeability of the phase to the absolute permeability (Anderson, 1987) (Honarpour and Mahmood 1988).

$$k_{rw} = \frac{k_w}{K} \; ; \qquad k_{ro} = \frac{k_o}{K} \tag{2}$$

2.3.1. Wettability effect on Relative Permeability

Wettability affects relative permeability because it is a major factor in the control of the location, flow, and spatial distribution of fluids in the core (Anderson, 1987). The oil relative permeability (k_{ro}) values are less at low water saturation in the mixed-wet case, because the oil is in competition with water in the large pores. Similarly, the water relative permeability (k_{rw}) at high water saturation is reduced in the water-wet case because the oil preferentially occupies the large pores (Ahmed, 2001).

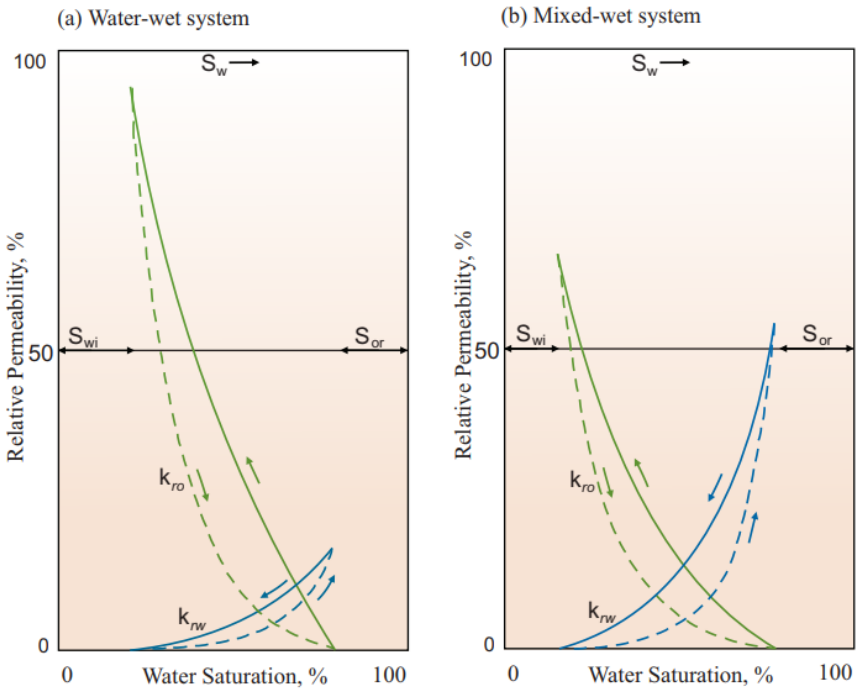

Figure 1. Schematic representation of relative permeability curves k_{ro} (green) and k_{rw} (blue) for (a) water-wet and (b) mixed-wet system. Modified from Donaldson (2008).

For a **water-wet core** as the preferentially wetting phase, water will be in the small spaces that were not invaded by oil whereas the oil will be in the large pores. When the waterflooding starts both phases flow. The oil relative permeability, k_{ro}, is high, since oil flows through the largest pores, and decreases as oil saturation decreases. The water relative permeability, k_{rw}, starts low and increases as water saturation increases.

In the sample, water saturation increases preferentially in the smaller pore spaces first, due to wetting forces. As the displacement moves from smaller to larger pores, the water increasingly occupies pore throats that were formerly filled with oil. One pore or a group of pores containing oil can become cut off from the rest of the oil and become trapped in place, due to driving pressure is not sufficient to overcome the capillary entry pressure. Eventually, all continuous flow paths are water-filled, and oil stops flowing. The final k_{rw} is lower than the original k_{ro} because of the oil trapped in large pores.

In a **mixed-wet core**, as before, initially k_{ro} is high and k_{rw} is low. However, as the water saturation increases, it invades the largest pores first and remains in the center of those pores, because of the oil-wet condition of the surfaces surrounding those pores. This causes a more rapid decline in k_{ro} as the most permeable paths fill with water. However, the water does not

trap the oil, because the oil-wet surfaces provide a path for the oil to escape from nearly water-filled pores (Abdallah et al., 2007).

It is worth to mention, although the Darcy equation (Equation 1) directly relates fluid flow rate to permeability, high permeability alone does not imply high flow rates passing through the core. Fluid viscosity (μ) also influences the flow rate, and more specifically the mobility of each phase given by Equations (2) and (3), respectively (Lyons, 1996).

$$\lambda_w = \frac{k_{rw}}{\mu_w}, \qquad \lambda_o = \frac{k_{ro}}{\mu_o} \tag{3}$$

Ideally, λ should be less than one to have a favorable mobility as the displaced phase (oil) has a higher mobility than does the displacing phase (water).

2.4. Capillary Pressure

The capillary pressure is defined as the difference between the pressures in each of the two fluids forming an interface (Glover, 2000). Generally, capillary pressure curves are obtained by displacing the wetting fluid with the nonwetting fluid (drainage). Then by displacing the nonwetting fluid with the wetting fluid (imbibition). In either case, the capillary pressure can be defined as:

$$P_c = (P_{nw} - P_w) \tag{4}$$

Where P_{nw} and P_w are the pressures of the nonwetting phase (water) and the wetting phase (oil), respectively. (Schlumberger, 2006). In this study, capillary pressure curves were obtained during an imbibition process by displacing the oil (wetting fluid) with water (nonwetting fluid) considering an oil-wet system/mixed-wet system.

2.4.1. Wettability Effect on Capillary Pressure

Wettability has been recognized as an important factor in remaining oil saturation and in capillary pressure and relative permeability curves (Anderson, 1987). Capillary pressure

curve shown in **Figure 2** depicts the capillary behavior of a water-wet, mixed-wet and oil-wet system initially saturated with water.

Figure 2a illustrates the capillary pressure behavior is depicted for a water-wet system. Segment 1, stated for primary drainage process, corresponds to the initial displacement when the water-saturated core is contacted by oil; an initial elevated pressure (P_T) known as threshold pressure of oil is required before oil will enter a water-wet core. As soon as P_T is exceeded, oil enters the core, displacing water. When the core is contacted by water at S_{wi} water will imbibe spontaneously into the core displacing oil. When the spontaneous imbibition reaches a limiting value, pressure must be applied to force water into the core and displace oil to a practical residual oil saturation (S_{wor}) as the capillary approaches a negative infinite value (i.e. segment 3). At S_{wor}, a threshold pressure (P_{to}) should be overcome before oil enter the core displacing water (i.e. segment 4).

Figure 2b shows the capillary pressure versus saturation relationships of a **mixed-wet core**. Some oil may imbibe into the core when it is contacted by oil at zero capillary pressure, after which pressure is required for injection of oil to displace water to S_{wi} (i.e segment 1).

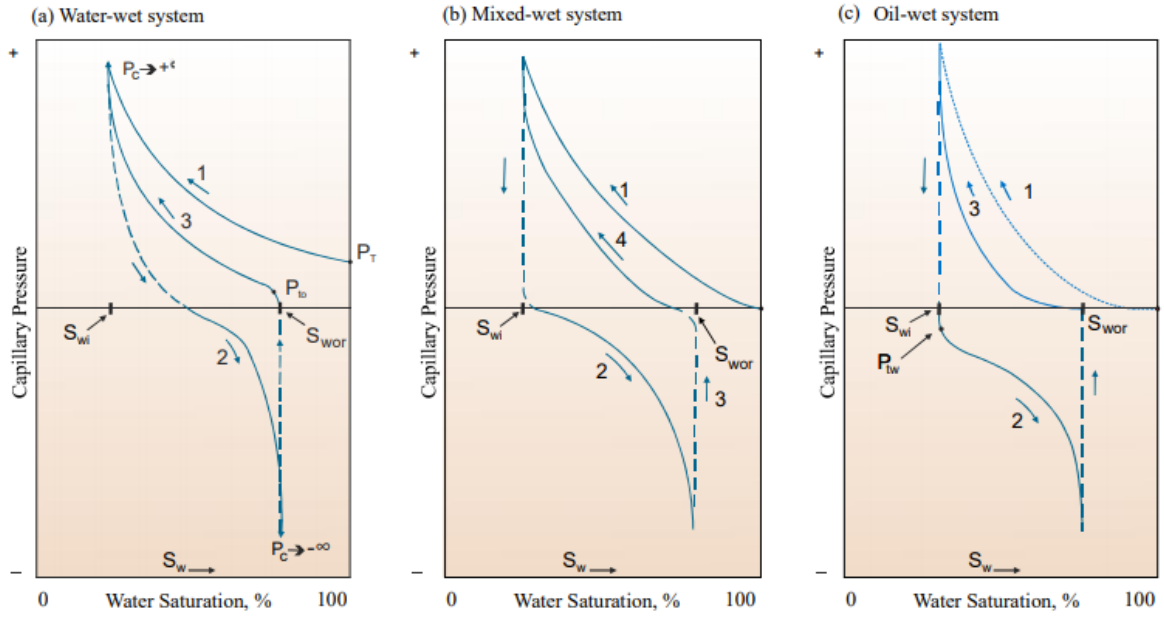

Figure 2. Illustration of the capillary pressure behavior for a (a) Water-wet, (b) Mixed-wet, and (c) Oil-wet system during drainage and Imbibition. Modified from (Donaldson & Alam, 2008).

With the saturation at S_{wi}, if the core is contacted with water, a small amount of water will spontaneously imbibe into the core until capillary pressure becomes zero (i.e. segment 2). Then, oil is displaced to its residual saturation (S_{wor}) as the water pressure is increased (i.e. segment 3). The capillary pressure is negative because the water injection pressure is greater than the oil pressure ($P_c = P_o - P_w < 0$). This whole process accounts for primary water imbibition, which is representative for the main experiment in this work.

Figure 2c depicts the capillary pressure behavior is depicted for an oil-wet system. When the water saturated core is contacted by oil, it will spontaneously imbibe some oil and displace water. Injection of oil will displace the water to S_{wi} (i.e. segment 1). At this point (when the core is contacted with water) will not spontaneously imbibe into the core. A threshold pressure (P_{tw}) is then required to overcome the repulsive forces to water. After P_{tw} is exceeded, oil will be displaced to S_{or} (i.e. Segment 2). At S_{or}, if the core is contacted with oil, oil will spontaneously imbibe into the core (i.e. Segment 3) (Donaldson & Alam, 2008).

2.5. Relative Permeability and Capillary pressure correlations

Corey (1954) and Skjaeveland et al. (2000) correlations were used for the estimation of relative permeability and capillary pressure.

Skjaeveland correlation given by **equation (34)**, is symmetrical with respect to the two fluids as neither of them dominates the wettability. Four parameters are used for this correlation. cw and aw, are constant parameters that define the positive part of the capillary pressure curve, while c_o and a_o, describe the negative part of the curve.

$$P_c = \frac{C_w}{\left(\frac{S_w - S_{wr}}{1 - S_{wr}}\right)^{a_w}} + \frac{C_o}{\left(\frac{S_o - S_{or}}{1 - S_{or}}\right)^{a_o}} \tag{5}$$

For relative permeabilities correlation, via **equation (35)** and **(36),** Corey assumes the wetting and non-wetting phase-relative permeabilities are independent of the saturations of the other phases as presented below:

$$krw = krw^{max} \left[\frac{S_w - S_{wi}}{1 - S_{wi} - S_{or}}\right]^{N_w} \tag{6}$$

$$kro = kro^{max}\left[1 - \frac{S_w - S_{wi}}{1 - S_{wi} - S_{or}}\right]^{N_o} \quad (7)$$

Where*:*

S_{wr} = Irreducible water saturation

S_{wi} = Initial water saturation

S_{or} = Residual oil saturation to water

$k_{rw\ (max)}$ = Water relative permeability at maximum water saturation

$k_{ro\ (max)}$ = Oil relative permeability at maximum water saturation

N_o = Corey oil exponent

N_w = Corey water exponent

3. Capillary Pressure End Effects

Capillary End Effects were intentionally highlighted during the core-flooding experiments in order to study capillary pressure and relative permeability undergoing these natural-occurring effects during unsteady-state experiments. In the section below will be explained further how this phenomenon occurs during waterflooding displacement experiments.

a. CEE - Description of the Phenomenon

Capillary End effect refers to a change in the capillary properties of a system at the time of relative permeability measurement. At the outflow face of the sample, however, there is a discontinuity in the capillary properties of the core, since the water passes abruptly from a region of relatively high capillary pressure (porous medium) into a void in which the oil-water interface has no sensible curvature, and the capillary pressure therefore vanishes (Osoba et al., 1951). Capillarity in the sample tends to draw the wetting phase into the core sample from the void, a tendency that must be overbalanced by the impressed pressure gradient if water is to pass from the core. Since part of the impressed pressure gradient goes to overcome the capillary pressure and hence is ineffective for overcoming frictional energy losses in the water, the water moves less rapidly than normally in the boundary (Richardson, et al., 1952). The water thus accumulates in the boundary grain layers, and the increased water saturation causes a decrease in the permeability to oil. According to Honarpour et al. (1986) this accumulation of the wetting phase at the outflow face of the sample creates a saturation gradient along the sample which disturbs the relative permeability measurements.

a. Pressure drop across the core

Since the nonwetting phase pressure is continuous at the inlet and the capillary pressure is constant at the outlet, it follows that the total pressure drop measured outside porous medium corresponds to the pressure drop in the nonwetting phase plus a constant value equal to the capillary pressure at the outlet.

For an imbibition process, both phase pressures are continuous at the outlet end since the capillary pressure there is zero. At the inlet boundary, the wetting phase pressure is

discontinuous. In this case, therefore, the pressure drop measured outside the core is equal to the pressure drop of the nonwetting phase through the core. (Virnovsky, Skjaeveland et al. 1995).

b. CEE depending on wettability

Figure below shows schematically the conditions existing in the three types of wettability cores, water-wet, mixed-wet and oil-wet when accounting for CEE at the outflow face during two-phase flooding experiment. In **Figure 3a** it is shown the saturation distribution with End Effects for each wetting states. There is saturation at equilibrium at the outlet of the core which is independent of the flow rate. **Figure 3b** illustrates Seq which corresponds to capillary pressure equal to zero for each wetting system. This Seq will vary between S_{wi} and (1 - S_{or}) saturation range depending on the wettability state. For a water-wet core it will be equal to S_{wi}, for an oil-wet core it will be closer to (1- S_{or}) and it will be placed in between for a mixed-wet core.

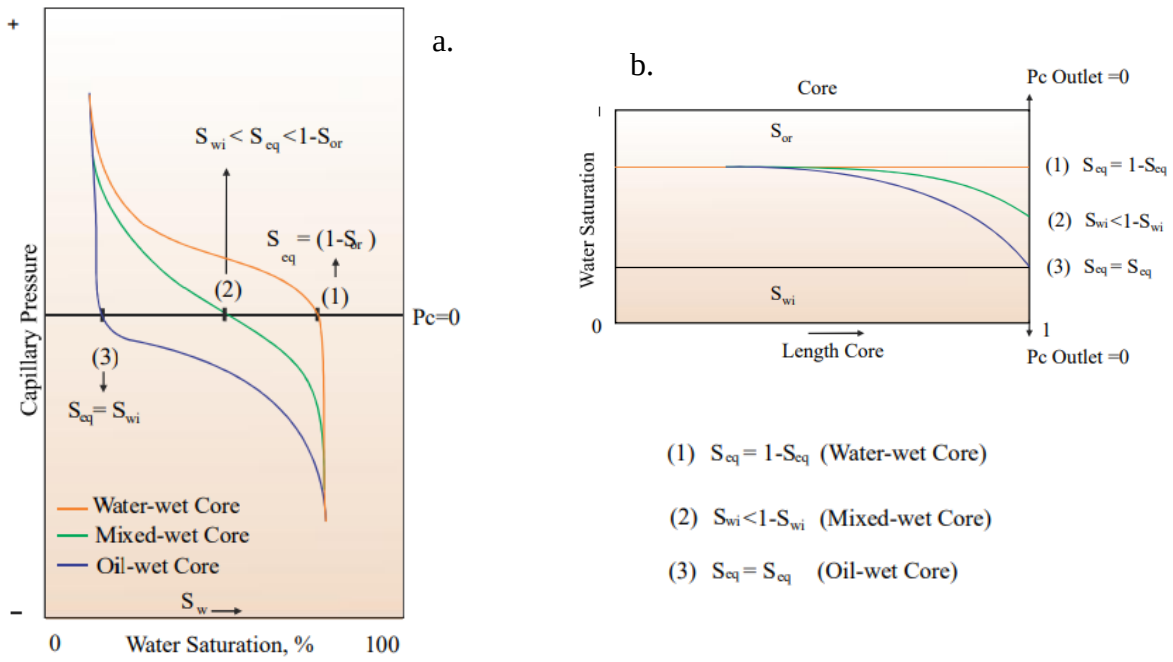

Figure 3. a) Capillary pressure and b) saturation distribution profile during two-phase flooding experiment with CEE in water-wet, mixed-wet and oil-wet conditions.

In an oil-wet case, the capillary pressure is negative, and there is no end effect at the inlet. Water saturation at the outlet, however, remains low, even after water breakthrough. Oil flows only when the viscous pressure gradient in water exceeds the capillary pressure gradient. In the final state both gradients are balanced. Heaviside et al. (1983) showed that Sor decreases slightly in an oil-wet core but the brine permeability increases significantly with an increase in flow rate. Some of the wetting fluid (i.e., oil) at the downstream end of the core is removed; hence, the brine permeability increases. On the other hand, for the mixed-wet case, capillary pressure is positive for low water saturation and negative for high water saturation. Most field mixed-wet cores are also weakly wet. Capillarity effects in a waterflood are similar to those of a weakly oil-wet rock (Mohanty and Miller, 1991).

c. Parameters promoting CEE

(Hinkley and Davis 1986) (Osoba, Richardson et al. 1951) drew the conclusion that short cores result in a greater influence of unwanted End Effects. (Kyte and Rapoport 1958) demonstrated that residual wetting phase saturation values determined by material balance was higher than the “true” value obtained with longer cores and higher flow rates.

According to (Kyte and Rapoport 1958) the end effect increases as the ratio of the capillary forces to the viscous forces in the system increases. They also illustrated the dependence of the End Effects on the viscosity of each of the phases, as it cannot be simply characterized by the viscosity ratio, and they concluded that end effect decreases as the viscosity of either component is increased.

(Kyte and Rapoport 1958) also support latter appreciations which agree the localized outlet end effect, will decrease as the length of the flooded system, the rate of injection, or the fluid **viscosities** are increased.

3.1. Mathematical Formulation for Core-flooding

The mathematical approach formulated by Andersen et al., 2017 will serve to study the core-flooding experiment at steady conditions. The model assumes incompressible multiphase flow for two phases (oil and water) to derive the total water influx based on Darcy's Law **(Equation 8)** and the mass transport equation **(Equation 9).** In this model gravity effect is neglected.

Let's denote o and w for the phases flowing in the porous medium.

Darcy´s Law:

$$u_i = -K\lambda_i \frac{\partial P_i}{\partial x}, \quad \lambda_i = \frac{K_{ri}}{\mu_i}, \qquad \text{and} \qquad \lambda_T = \lambda_o + \lambda_w \; ; \quad (i = o, w) \tag{8}$$

And conservation of mass gives:

$$\frac{\partial u_i}{\partial x} + \Phi \frac{\partial S_i}{\partial t} = 0, \qquad (i = o, w) \tag{9}$$

Where: u_i is Darcy velocity, K absolute permeability, P_i pressure, k_{ri} relative permeability, μ_i viscosity and S_i saturation, λ_i.mobility,

By using capillary pressure function, $P_c = P_o - P_w$, and total Darcy's velocity $u_T = u_w + u_o$, the total flux given by **Equation (8)** takes the form:

$$u_T = u_w + u_o = -K\lambda_w \frac{\partial P_w}{\partial x} - K\lambda_o \frac{\partial P_o}{\partial x} = -k(\lambda_T - \lambda_o)\frac{\partial P_w}{\partial x} - K\lambda_o \frac{\partial P_o}{\partial x}$$

$$u_T = -K\lambda_o \frac{\partial (P_o - P_w)}{\partial x} - K\lambda_T \frac{\partial P_w}{\partial x}$$

$$u_T = -K\lambda_o \frac{\partial P_c}{\partial x} - K\lambda_T \frac{\partial P_w}{\partial x} \tag{10}$$

Taking the relationship $(S_o + S_w) = 1$ and by replacing **Equation (10)** in transport **Equation (9)** it gives:

$$\frac{\partial u_T}{\partial x} = 0 \; ; \tag{11}$$

From **Equation (10**), the pressure gradient $\frac{\partial P_w}{\partial x}$ can be rearranged to be:

$$\frac{\partial P_w}{\partial x} = -\left(\frac{u_T + K\lambda_o \frac{\partial P_c}{\partial x}}{K\lambda_T}\right) \tag{12}$$

By inserting **Equation (12),** the mass balance of water phase $\left[(\emptyset \frac{\partial S_w}{\partial t} = -\frac{\partial u_w}{\partial x}\right]$ can be written as:

$$\emptyset \frac{\partial S_w}{\partial t} = \frac{\partial}{\partial x}\left(-f_w u_T - K f_w \lambda_o \frac{\partial P_c}{\partial x}\right) \tag{13}$$

Where f_w is the fractional flow

$$f_w = \frac{\lambda_w}{\lambda_T} = \frac{\lambda_w}{\lambda_w + \lambda_o} \tag{14}$$

Since (Buckley & Leverett, 1942) equation neglects capillary pressure. **Equation (13)** turns out to:

$$\emptyset \frac{\partial S_w}{\partial t} = -u_T \frac{\partial}{\partial x}(f_w) \tag{15}$$

Mathematical Definition of Capillary End Effect

The model assumes that water is injected in the negative direction, starting from x = ∞ (inlet) towards x = 0 (outlet). Then u_T is considered to be negative and is known and equal to u_w as water is injected to core. The boundary conditions at the inlet and outlet are given by **Equation (16)** and **(17):**

$$f_w(x = \infty) = 1, \quad \left.\frac{\partial P_c}{\partial x}\right|_{x=\infty} = 0 \tag{16}$$

The capillary effect is defined as zero capillary pressure at the boundary at the outlet, then:

$$P_c|_{x=0} = 0 \tag{17}$$

Assuming Steady State Conditions

As there are no changes with time for steady state then we have:

$$\partial_t S_i = 0, \quad \partial_t P_i = 0, \quad i = (o, w) \tag{18}$$

By replacing steady-state equation (**Equation 18**) into the mass balance of water phase (**Equation 13**), then water saturation as a function of spatial coordinate ($S_w = S_w(x)$) can be written as:

$$0 = \frac{\partial}{\partial x}\left(-f_w u_T - K f_w \lambda_o \frac{\partial P_c}{\partial x}\right) \tag{19}$$

Finally, by integrating (**Equation 19**) we can obtain the inlet influx of water:

$$u_T = f_w u_T + K f_w \lambda_o \frac{\partial P_c}{\partial x} \tag{20}$$

The mathematical definition for the water influx is composed of two terms, the advective to the right and the capillary diffusion to the left side of the expression. Those terms allow to describe the non-uniform distribution of the phases.

By using water mobility definition $\lambda_w = \frac{k_{rw}}{\mu_w}$ the saturation gradient along the core can also be derived from (**Equation 20**):

$$\frac{\partial S_w}{\partial x} = \frac{u_T u_w}{K} \frac{1}{Pc\,(S_w)\; k_{rw}(S_w)} \tag{21}$$

Experimental core-flooding under steady conditions in this study can be mathematically modeled through analytical formulation from Andersen et al., 2017.

4. Material and Preparation

Preliminary preparations for further work are described in this section. Establishment of initial saturation state, wettability alteration, and flooding experiments will be outlined in section 5.

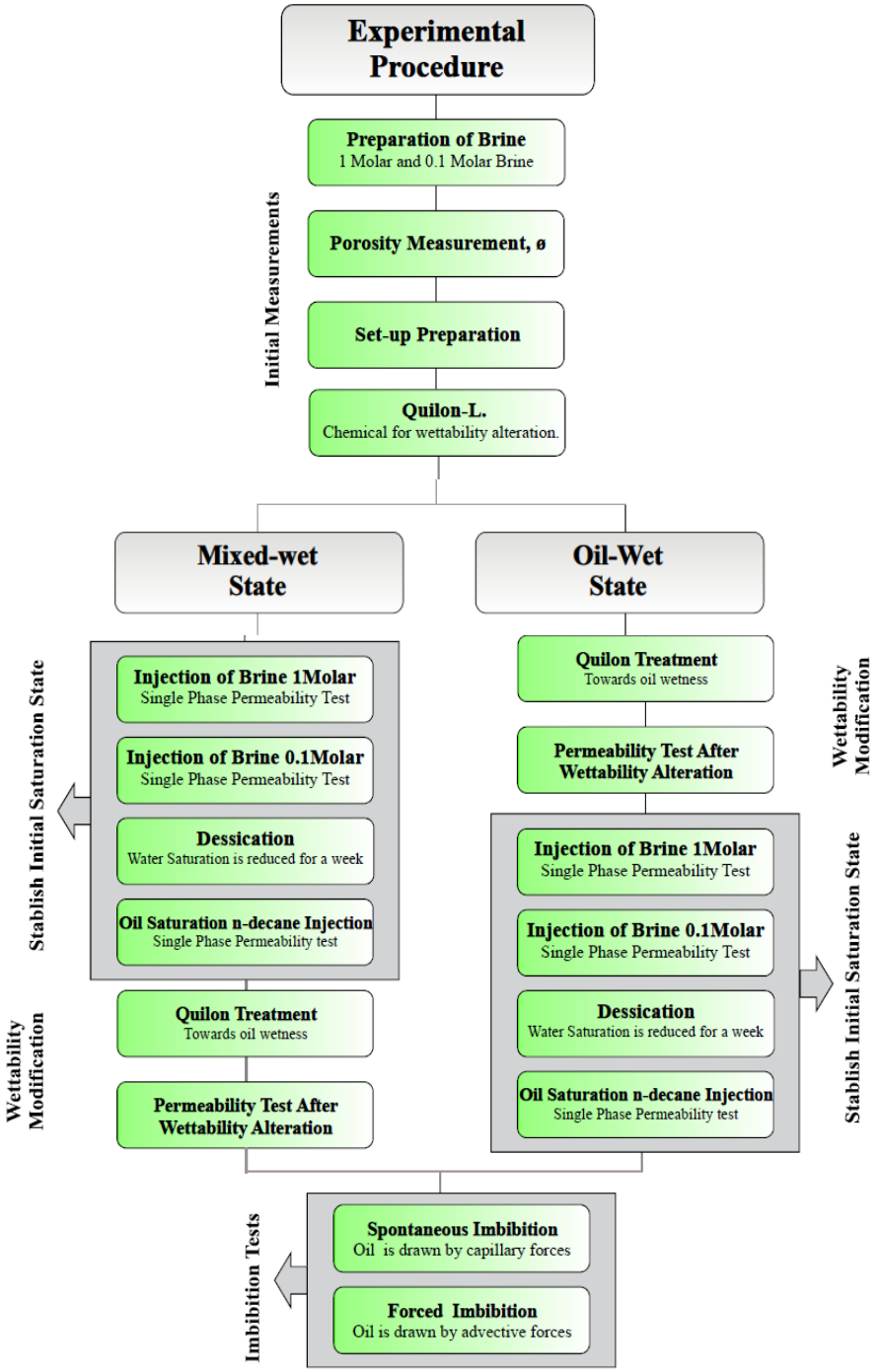

Figure 4. Flow chart showing full experimental procedure to conduct Spontaneous and Forced Imbibition on strongly water-wet Sandstones.

Figure 4 presents a flow diagram for the various tests carried out on every core sample. In general, cores were aged towards more oil-wet conditions, followed by a spontaneous imbibition test. During this test, oil produced vs time was recorded. Then, a forced imbibition test was performed at a constant rated followed by a systematic increment in rate. Pressure drop and oil production vs time was also measured throughout the experiment.

4.1. Core Type

Bentheimer Sandstone outcrop samples are considered to be ideal for laboratory studies due to their lateral continuity and block scale homogeneous nature (Peksa et al. 2015). Both under natural and thermally altered conditions, it has a limited amount of minerals, a constant grain size distribution, porosity, permeability, and dielectrical values, which makes it suitable for standard laboratory experiments and comparison with theory. Over the years they have been used to investigate reservoir topics ranging from passive and active properties of oil/gas/water/rock interaction, flowing processes, and transport (Peksa et al., 2015).

4.2. Oil and Brine

NaCl (1 mol/L) - 6.23 slightly acidic - was used as a Brine. 58.44 grams of Sodium Chloride were dissolved in 1 Liter of solution (Distilled water plus sodium Chloride). It was mixed overnight and filtered by using 0.22 µm filter paper to get a clear solution for following flooding. Density of the Brine was measured in a density-meter Anton Paar model DMA 4100M calibrated with water.

Table 1. *Properties for 0.1M and 1M Sodium Chloride used during core flooding. Extracted from Sodium Chloride data-sheet, (2018).*

	Sodium Chloride Brine		
Properties	**0.1M NaCl**	**1M NaCl**	**Units**
pH	6.23	6.23	
Density	1.00189	1.0386	g/ml
Specific Gravity	1.0037	1.0405	
Viscosity	1.008	1.09	cp
Appearance	Colorless Liquid		

Concentration of NaCl Brine 1Molar (M) was diminished to 0.1 M to be injected in the core and establish initial saturation state. Brine concentration was reduced to 0.1M by diluting 100 mL of Brine in 900 ml of Distilled water. ***NaCl (***1 mol/L) - 6.23 slightly acidic - was used as a Brine. 58.44 grams of Sodium Chloride were dissolved in 1 Liter of solution (Distilled water plus sodium Chloride). It was mixed overnight and filtered by using 0.22 µm filter paper to get a clear solution for following flooding. Density of the Brine was measured in a density-meter Anton Paar model DMA 4100M calibrated with water.

Table 1 shows the properties for both brines.

N-decane (GC area ≥ 94%) was used as the oil phase and was employed in the preparation of the solution for wettability alteration. Properties of n-decane are presented in **Table 2**.

Table 2. *Main properties of n-decane.* Taken from n-decane data-sheet, (2018).

n-decane Properties		
Properties	**Value**	**Units**
Molecular Weight	142.29	g/mol
Solubility	0.00005	g/l
Boiling Point (174°C)	1013	mbar
Density (20°C)	0.73	g/ml
Viscosity	0.92	cp

4.3. Chemical for wettability modification

Quilon L and H (3 % wt) were used to change the wettability of the cores. Quilon is a dark green solution developed by Zaclon® that reacts chemically with polar groups on negatively charged surfaces (Quilon data sheet, 2016). The fatty acid chains in this solution are directed away from the particle's surface imparting the water repellent properties, without affecting the porosity of the core (Maini, et al. 1986).

Multiple grades of Quilon are offered (i.e. H, L, C, S, and M). Quilon® H and L are about 60% more concentrated than C, M, and S. Both, L and H grades have similar chemical properties such as boiling point, melting point, and density (

Table 3) (Quilon data sheet, 2016). However, Quilon L was found to be soluble in water and n-decane, which lead to better results when tested on the cores. It is important to mention that the Quilon L bottle used in this experiment was opened in 2014. However, there was no evidence for anomalous results.

Table 3. Properties for both grades of Quilon, L and H used for the wettability modification of the samples. Taken from Quilon data sheet, (2016).

Properties of Quilon

	Quilon L	**Quilon H**	**Units**
Concentration	8.5 - 9.5	8.5 - 9.5	wt. % Cr in Isopropanol
Boiling point	82°C	82°C	°C
Melting point	4 °C	2 °C	°C
Density	1.025	1.015	g/ml at 25°C

4.4. Experimental Set-up

Two horizontal core holder set-ups were used to perform the core-floodings. Both core holders were set to a back pressure of **6.5 bar** (± 1 Bar) at the inlet end and a confining pressure of **27 bar** (± 2 bar). The core holders were connected to two differential pressure ROSEMOUNT® transducers (model 3051CD1A22A1BM5L4) at the inlet and outlet end (

Figure *6*). Pressure drop data was constantly monitored by a computer.

The range of differential pressure measured by the transducer varied from 0 to 2.5 bar for the highest and 0 to 62.16 mbar for the lowest. A Quizix pump (QX PUMP) from AMETEK CHANDLER ENGINEERING with double piston cylinders was used to inject fluids into the core. A graduated burette, which is part of the water/oil separator arrangement, was placed after the back-pressure regulator to measure oil and water production **(Figure 5)**. Both fluids enter the burette through the bottom and the oil volume can be read at the top as oil is

separated by gravity; water is drained to a water collector. Experiments are carried out at atmospheric temperature.

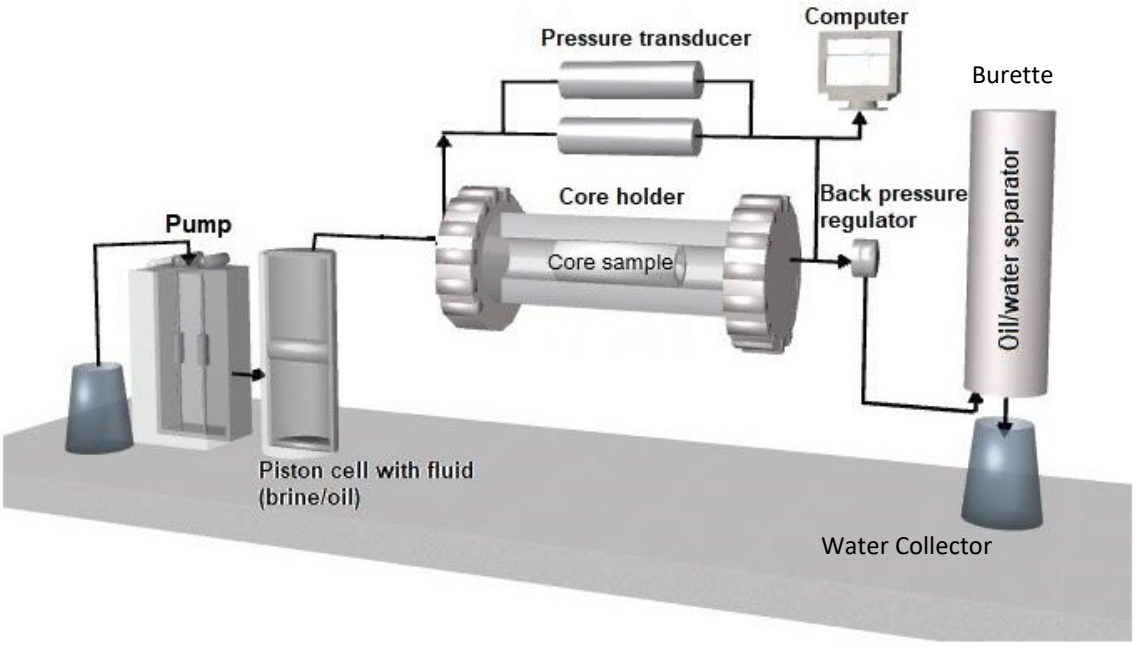

Figure 5. Schematic illustration of the rig piping used for permeability tests and the two-phase core-flooding to verify capillary End Effects.

The set-up used for the permeability test of **OWB_3** slightly differs from the main set-up depicted above which was used for all procedures. The pump is a low bracket GILSON pump (model 307) and the one-off pressure transducer used varies within a range of 0 to 2486.42 mbar.

4.5. Forced Imbibition Experiment Design

When designing a core-flooding experiment, the primary concern is to eliminate or reduce CEE to the lowest and, hence, obtain accurate curves for Pc and RelPerm. However, this experiment is especially designed to magnify such CEE in the core samples. The requirements to induce CEE during core-flooding tests are numbered below:

a. **Unsteady state method.** Unsteady-state and steady-state displacement experiments are commonly used for relative permeability measurement. The unsteady-

displacement method is the most common because it is fast and qualitatively resembles the flooding process in field conditions. It is an indirect method since relative permeabilities are calculated instead of measured. On the other hand, the steady-state method is time consuming and in most cases does not resemble the displacement process, which involves movement of saturation fronts. (Mohanty and Miller 1991). More importantly, during steady-state experiments, End Effects are reduced or eliminated (Honarpour and Mahmood 1988)). The unsteady-state method will be effectively employed in this study as it tends to undergo capillary End Effects at the entrance and exit of the core, especially when low rates are used.

b. **Low flow rates.** When the flooding is carried out at lower rates, higher accumulation of the wetting phase prevails at the exit of the core (Hinkley and Davis, 1986; Osoba, et al., 1951). Thus, oil can be gradually pushed out of the core as long as advective forces, given by increasing flow rates, are strong enough to overcome capillary forces that hold the oil back. Conversely, if floods are carried out at high flow rates, the trapping mechanisms in the core are less effective and most of the oil will be produced at once.
c. **Oil wetness characteristics** cause accumulation of the wetting fluid (oil phase) in the core. Therefore, flow rates (i.e. advective forces) in oil-wet and mix-wet cores must be increased to take out the oil that is left behind. In a water-wet core, End Effects are generally negligible. If floods are carried out on water-wet cores, especially at high rates, the capillary forces inducing oil trapping mechanisms will not take place.
d. **High Permeability.** Permeability of the selected rock analogues are high enough to generate high pressure drops across their length. It will assure a broad range of pressure drops to systematically produce the oil.
e. **Short cores** and **low water viscosity** also facilitate the occurrence of CEE during core-flooding experiments as explained by Kyte and Rapoport (1958) and Hinkley and Davis (1986) A lower water viscosity makes it suitable for this study since water will have lower resistance to flow and will selectively migrate through the oil-invaded region (fingering) at the end of the core, promoting increased oil saturation at the outlet. Simultaneously, the comparatively higher resistance of oil to flow in the water-

invaded region will cause oil to accumulate in the direction of increasing pressure, broadening the size of the oil-bearing region in the core (Kyte and Rapoport 1958).

5. Experimental Tests and Procedure

This section will introduce the experimental tests and procedure followed in the study. The whole experimental procedure was performed for both a mixed-wet Bentheimer (MWB_2) and an oil-wet Bentheimer (OWB_3) sample. For MWB_2, initial saturation state was stablished before wettability alteration. Conversely, for OWB_3, initial saturation was reached after wettability process since the core sample should be dry for that procedure.

An initial trial consisted of two additional samples, an oil-wet Berea (OWBEREA) and a first mixed-wet Bentheimer (MWB_1). Although, these trials could not be finished, they provided valuable insight for the following work. Experimental tests on the MWB_1 sandstone had to be repeated after getting unexpected results in wettability treatment. MWB_2 was its second attempt. OWBEREA could not be finished as oil was produced during a high pressure drop event. Main observations of these early attempts are reported in appendix in figure.

5.1. Porosity and Pore volume measurements

An imbibition test was performed in order to calculate porosity in the core samples. Each sample was immersed into a vacuum chamber protected by a same-size plastic container. The air remaining in the core was removed by vacuuming (

Figure *6*). Then, 1M brine (wetting fluid) was flowed inside the core until filling up the container and left for 24 hours. Each sample was weighted before and after imbibition to measure the weight of dry and saturated cores.

Pore volume (PV) (i.e. volume of fluid), and porosity were calculated **via Equation (22)** by using the bulk volume and the weights previously measured. Bulk Volume was computed via **Equation 23** using the dimensions of the core measured with a Vernier caliper. All these parameters are shown in **Table 5** presents the results for porosity and pore volume measurements in MWB_1, MWB_2, OWB_3 and OWBEREA samples through imbibition method as described in **section 5.1.**

Table 5. Parameters of MWB_1, MWB_2, OWBEREA and OWB_3 core plugs used for calculating porosity and pore volume.

Properties of Core Samples

	MWB_1	MWB_2	OWBEREA	OWB_3	Units
Diameter (D)	37.79	37.81	37.72	37.74	mm
Length (L)	89.89	90.03	89.24	90.03	mm
V_{Bulk}	100.82	101.08	99.72	100.71	ml
m_{dry}	203.36	205.3	202.91	205.24	g
m_{sat}	227.57	228.85	224.39	227.26	g
m_{brine}	24.21	23.55	21.48	22.02	g
PV	23.31	22.68	20.68	21.98	ml
ρ_{brine}	1.0386	1.0386	1.0386	1.0386	g/ml
φ	23.12	22.44	20.74	22.15	%

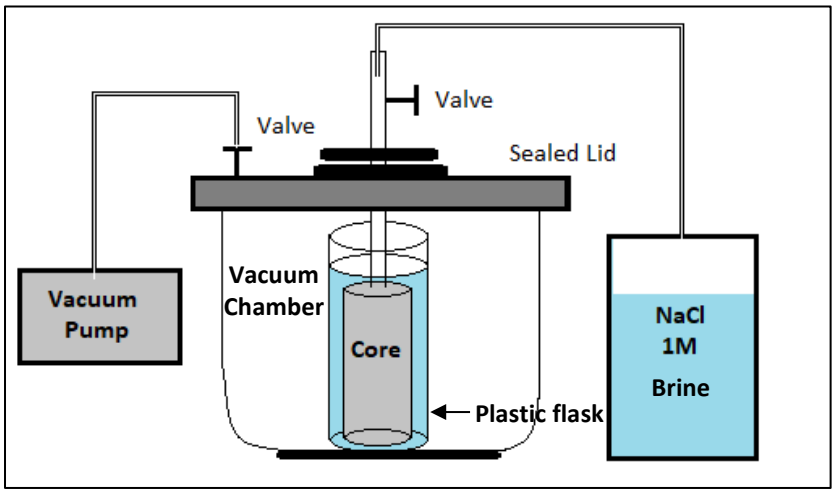

Figure 6. Schematic illustration of the Imbibition set-up used for core saturation with 1M Brine.

$$\varphi = \frac{V_{Pore}}{V_{Bulk}} = \frac{V_{brine}}{V_{Bulk}} = \frac{{m_{brine}}/{\rho_{brine}}}{V_{Bulk}} = \frac{{(m_{Sat} - m_{Dry})}/{\rho_{brine}}}{V_{Bulk}} \quad (22)$$

Where: V_{Fluid} = Volume of Brine representing the pore volume (ml)
V_{Bulk} = Bulk Rock volume (ml)
m_{brine} = Mass of Brine (g)
ρ_{brine} = Density of the Brine (g/ml)
m_{Sat} = Mass of saturated core (g)
m_{Dry} = Total dry mass of the core (g)

$$V_{Bulk} = \frac{\pi}{4} \times D^2 \times L \quad (23)$$

5.2. Permeability Tests Initial Saturation State

During the permeability tests, fluids were injected through the core at increasing and decreasing flow rates, varying from 0.25 to 0.5 ml/min. A differential pressure (dP) was induced along the length of the core, caused by the difference in pressure between inlet and outlet. Fluids were continuously injected until pressure drop was stabilized. That indicated that the equilibrium in the core was stablished.

Permeabilities were calculated during injection of 1M and 0.1 M brine and n-decane by using Darcy's Law. Simultaneously, initial saturation state was stablished by injecting 0.1 M NaCl Brine and n-decane through every core. Permeability results were validated by performing the tests twice in the cases where dP values were suspicious or just deviated from the trend. Every flooding procedure will be described below. Corresponding rate vs pressure drop profiles are presented in ***Appendix 1.***

1. *Absolute Permeability of water* – Each core sample was mounted in the core holder and 1M Brine was pumped through the core at different flow rates until reaching stabilized

pressure drop. Afterwards, 5 PVs of 0.1 M Brine were pumped continuously to displace 1M brine previously injected in the core. The flow rate used was 0.5 ml/min. During this flow, the pressure drop varied according to the change in brine viscosity, according to Darcy's Law.

2. *Initial water saturation, (S_{wi})* - To establish initial water saturation, each core was saturated with 0.1M NaCl brine and subsequently weighted. Following, water saturation was diminished by evaporation trough desiccation until obtaining approximately 10% of residual water saturation. 0.1M brine was concentrated back to 1M in the process. Initial saturation state and mass measurement for every core can be seen in **Table 7**.
3. *Effective Permeability of Oil, (k_o)* - After S_{wi} was reached in the core, 5 PVs of n-decane were injected through the core to calculate effective permeability of oil and to establish the Initial Oil Saturation (S_{oi}). A piston cell was used to pump n-decane and avoid contact with the pump itself. A small portion of water was produced at the beginning of the flooding with meaningless effects in the initial saturation procedure. Effective permeability test was carried out before and after mixed-wettability process. After wettability alteration of mixed-wet cores, the permeability test was carried out during the flush out of Quilon Solution.
4. *Permeability calculation*. Linear regression of dP vs rate was plotted and permeability was calculated by Darcy's Law given by **Equation (24)**. As an example, linear regression for dP vs rate for a core sample is presented in **Figure 7**. System unit were implemented accordingly.

$$k = Q\ \mu_{brine} \frac{L}{A(P_i - P_o)} \tag{24}$$

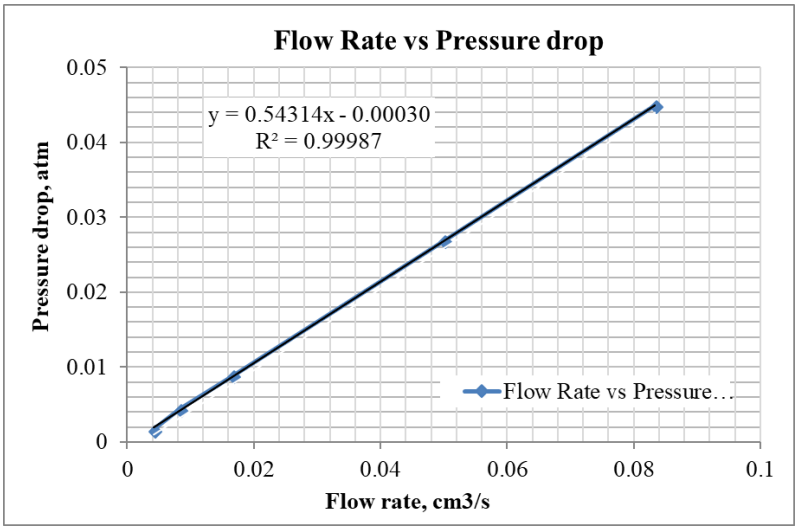

Figure 7. Example of linear regression of Pressure drop vs rate for a core during 1M flooding.

5.3. Wettability Alteration Treatment

For the purpose of this study, wettability of the cores was artificially turned into oil-wetness conditions (i.e. mixed-wet and oil-wet). Two samples underwent a wettability change process to be artificially turned into a Mixed-wet Bentheimer (MWB_2) and Oil-wet Bentheimer (OWB_3). The wettability change procedure slightly differed depending on the pursued wetting state. Quilon solution was dissolved in water when oil-wet conditions were pursued, while Quilon was dissolved in n-decane when mixed-wet stated was targeted.

A first attempt of wettability modification on the MWB_1 sample was made by using Quilon H however, final results were not expected. Results are presented in **section 6.3** This sample was not tested further following the attempted wettability alteration.

5.3.1. Wettability modification for MWB

The wettability technique applied for obtaining mixed-wet core was mentioned by (Abeysinghe et al., 2012). The number of pore volumes injected were given by the effluent color and stabilization of pressure drop. When dark coloration was detected at the effluent, it dictated that n-decane had been displaced by Quilon solution. In contrast, lighter coloration at the effluent spoke that Quilon had been flushed out. Time was controlled in order to guarantee that the procedure was not interrupted. If interrupted, the process would have to be started over as the Quilon solution could be degraded within the core. Contact with air and light should also be minimized.

a. Preparation of solution

The solution was prepared by mixing Quilon L in n-decane (3 wt%). The mixture was stirred and filtered using 0.45 μm filter paper. Exposure with air or light were avoided during preparation by keeping the containers closed and also by covering the equipment and flow lines with aluminum foil. After filtering the solution, it was transferred to a piston cell to start the injection. Fresh solution was prepared for injection in the second direction.

b. Injection in the First direction

Before starting injection of Quilon L, the sample was drained by vacuum and saturated with brine and n-decane to stablish initial saturation. The core was mounted horizontally in the core holder, and injection of Quilon solution was started in in the first direction at a constant rate of 0.5 ml/min. No water was produced at this stage. Dark coloration in the last effluent confirmed adsorption of Quilon. Thus, injection was stopped, and direction was reversed.

c. Injection in the reversed direction

The core was rotated upside down 180° in the horizontal direction, taking care that it was not twisted over its horizontal axis. This rotation assures a homogenous distribution of the solution through the core as seen in **Figure 8**. Note that in this step core surfaces that were not covered in the first injection are now in contact to the chemical in the second direction.

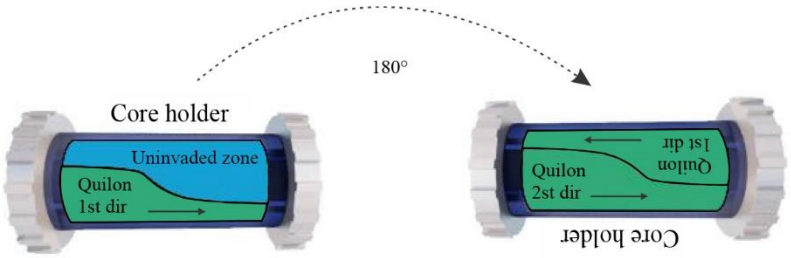

Figure 8. Profile for invasion of Quilon solution into the core and core holder rotation for injection of Quilon in a) 1st direction and b) 2nd direction.

d. n-decane Injection

With the core holder still oriented in the second direction of Quilon injection, n-decane was pumped through the core to remove the excess of treatment chemicals. One hour was allowed before injection of n-decane.

5.3.2. Wettability modification for OWB_3

The basis for wettability modification of OWB_3 was proposed by (Tiffin and Yellig, 1983) and was applied for wettability alteration of strongly water-wet Berea sandstones by (Maini et al., 1986) and (Askarinezhad et al., 2017). The solution used for wettability alteration of this sample was made by dissolving Quilon L (3 wt%) in distilled water. Foam was produced while dissolution and filtering of the solution. The dry core sample were mounted in a core holder and 28 bar (± 2 bar) overburden pressure was applied. The core was vacuumed and saturated with the filtered Quilon-L solution. The sample stayed vertically oriented onto the

core holder (**Figure 15c)** while five Pore Volumes (PVs) of the solution were pumped upward at 0,5 ml/min. Then, the core was turned upside down and injection was reversed. After that, the samples were demounted and taken to a dark, 95°C hot oven for a week. After the treatment, the sample was well-wrapped with cellophane sheets and stored in a dark storage compartment to avoid exposure to air and prevent oxidation. Berea sample was treated previously as part of the work carried out by (Askarinezhad et al., 2017), that was provided to conduct further experiments.

5.4. Spontaneous Imbibition Test

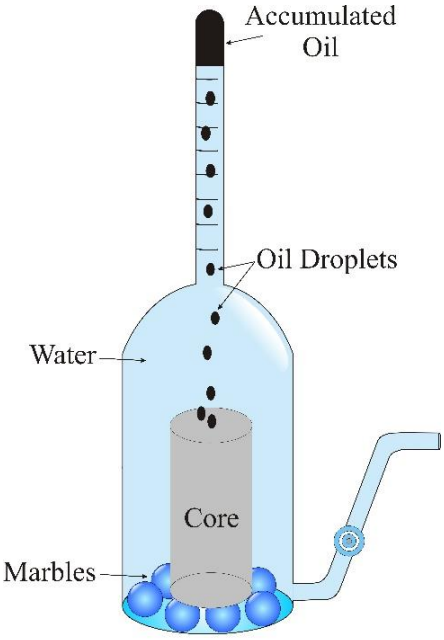

After wettability alteration, MWB_2 was stored in n-decane to be preserved before spontaneous imbibition. OWB_3 was taken out immediately from core holder to the spontaneous imbibition cell.

The individual samples were immersed in an Amott cell already filled up with 1M brine as shown in **Figure 9**. Marbles were set at the bottom of the cell to allow brine to imbibe through the base of the core.

Figure 9. Amott cell for spontaneous imbibition, the core is placed inside, and water is allowed to imbibe spontaneously.

The principle around this method is that the water acting as the nonwetting fluid is replaced by the oil (wetting fluid) that spontaneously imbibe into a core until capillary pressure equals to zero. That phenomenon occurs because of the action of capillary forces inside the core. As long as brine imbibes into the sample, oil droplets are released from the core and get accumulated at the top of the cell to be measured as presented in **Figure 9**.

5.5. Forced Imbibition

Having met the specifications stated in **Section 4.7**, the core floods were carried out at atmospheric temperature. After establishing a new initial saturation (S_{wi}, *FI*) (i.e. after spontaneous imbibition), every sample was mounted in the core holder under confining pressure of 29 mbar. An inert blue dye was added to the oil phase (n-decane) to be injected in the core and differentiate between oil and water. It also allowed and easy track of the location of oil in the core-flooding set-up. Water was injected in the core at low rates, and oil and water were produced at the outlet. In each core, flow rate was gradually increased (**Table 4**) immediately after reaching steady conditions in both pressure drop and oil production. Steady state conditions in this case refer to stabilized differential pressure and oil production after a flow rate increment. Initial rate for each core started at 0.6 PV/day and was increased by a factor of two (**Table 4**). The largest flow rates used for both OWB_3 and MWB_2 were constrained due to the pump's limited capability (7.5 ml/min).

Table 4. *Flow rate increments during forced Imbibition for OWBEREA, MWB_2, and OWB_3.*

	OWBEREA		***MWB_2***		***OWB_3***	
PV	20.84 ml		22.02 ml		21.98 ml	
Flow Rates	PV/day	ml/min	PV/day	ml/min	PV/day	ml/min
Q1	0.20	0.0029	0.40	0.0061	0.40	0.0061
Q2	0.40	0.0058	0.60	0.0092	0.60	0.0092
Q3	0.60	0.0087	1.20	0.0184	1.20	0.0183
Q4	1.20	0.0174	2.40	0.0367	2.40	0.0366
Q5	2.40	0.0347	4.80	0.0734	4.80	0.0733
Q6	4.80	0.0695	9.60	0.1468	9.60	0.1465
Q7	9.60	0.1389	19.20	0.2936	19.20	0.2931
Q8	19.20	0.2779	38.40	0.5872	38.40	0.5861
Q9	38.40	0.5557	76.80	1.1744	76.80	1.1723
Q10	76.80	1.1115	153.60	2.3488	153.60	2.3445
Q11	153.60	2.2229	307.20	4.6976	307.20	4.6891
Q12	307.20	4.4459	490.46	7.5000	491.36	7.5000
Q13	518.24	7.5000	-	-	-	-

5.6. Numerical Simulation

Numerical simulations were carried out by using Sendra Software. This simulator uses a fully implicit black oil formulation based on Darcy's Law and continuity equation (Sendra, 2016) with an automated history matching approach (estimation mode) and a forward simulation of an experimental scenario (simulation mode). Both modules were implemented in this study. This simulator was chosen due to its versatility for two-phase core-flooding experiments to estimate RelPerm and Pc curves based on history matching of pressure drop and oil production.

Water and oil relative permeability curves were estimated by using Corey correlation (Corey, 1954) given by **Equation (5)**. The correlation proposed by (Skjaeveland et al., 2000) was implemented for obtaining Capillary pressure data via **Equation** (6).

Relative permeability end points, $k_{rw\,(Sor)}$ and $k_{ro\,(Swi)}$, obtained from permeability experiments were defined for the simulation. $k_{rw\,(Swi)}$ and $k_{ro\,(Sor)}$ were assumed to be zero. The curvature for water relative permeability and oil relative permeability was shaped by varying the N_w and N_o Corey parameters. For the Pc curve, the four parameters in Skjaeveland et al. (2000) correlation were modified. C_w and a_w parameters were imputed to define the positive part of the capillary pressure curve, while Co and a_o shaped the negative part of the capillary pressure curve.

Rock and fluid properties, bump rates, and simulation time were defined as the initial input for the simulation model. Experimental data of pressure drop and production vs time were also included in the model. A core sample with 100 grids was used by default in Sendra.

Remarks. Actual oil production was calculated by subtracting the dead volume (oil left behind in the pipeline between the outlet of the core and the top of the burette) from the total oil production. Additionally, S_{wi} for Pc and RelPerm correlations was based on water saturation after desiccation. However, initial water saturation (S_{wi}) for flooding was based on saturation after spontaneous imbibition.

6. Results and Discussion

6.1. Porosity and Pore volume measurements

Table 5 presents the results for porosity and pore volume measurements in MWB_1, MWB_2, OWB_3 and OWBEREA samples through imbibition method as described in **section 5.1.**

Table 5. Parameters of MWB_1, MWB_2, OWBEREA and OWB_3 core plugs used for calculating porosity and pore volume.

Properties of Core Samples

	MWB_1	**MWB_2**	**OWBEREA**	**OWB_3**	**Units**
Diameter (D)	37.79	37.81	37.72	37.74	mm
Length (L)	89.89	90.03	89.24	90.03	mm
V_{Bulk}	100.82	101.08	99.72	100.71	ml
m_{dry}	203.36	205.3	202.91	205.24	g
m_{sat}	227.57	228.85	224.39	227.26	g
m_{brine}	24.21	23.55	21.48	22.02	g
PV	23.31	22.68	20.68	21.98	ml
ρ_{brine}	1.0386	1.0386	1.0386	1.0386	g/ml
φ	23.12	22.44	20.74	22.15	%

6.2. Permeability Tests and Initial Saturation State

Permeability results performed in all samples will be outlined in this section. Besides, initial saturation state **Table 7** is also presented as it was performed during the permeability tests. Permeability procedures for MWB_2 and OWB_3 were supported by main observations obtained from the MWB_1 and OWBEREA attempts presented in ***Appendix 1***

Table *6* summarizes the permeability results obtained for every sample. Permeability tests for MWB_2 were carried out before wettability treatment. Whereas for OWB_3, they were performed after wettability alteration since the sample should be dry for changing the wettability.

Permeability	**MWB_1**	**MWB_2**	**OWBEREA**	**OWB_3**
K at S_{wi} (1M)	3.20	3.01	0.63	3.13
K at S_{wi} (0.1M)	3.13	2.98	0.63	3.06
Permeability before Wettability alteration				
$k_{ro\ (Swi)}$	0.98	1	-	-
$k_{rw\ (Sor)}$	-	0.03	-	-
Permeability after Wettability alteration				
$k_{rw\ (Swi)}$	0	0	0	0
$k_{ro\ (Swi)}$	0.98	0.46	0.64	0.73
$k_{rw\ (Sor)}$	-	0.03	0.72	0.50
$k_{ro\ (Sor)}$	0	0	0	0

Table 6. Permeability results obtained for the four samples MWB_1, MWB_2, OWBEREA and OWB_3.

Permeability	**MWB_1**	**MWB_2**	**OWBEREA**	**OWB_3**
K at S_{wi} (1M)	3.20	3.01	0.63	3.13
K at S_{wi} (0.1M)	3.13	2.98	0.63	3.06
Permeability before Wettability alteration				
$k_{ro\ (Swi)}$	0.98	1	-	-
$k_{rw\ (Sor)}$	-	0.03	-	-
Permeability after Wettability alteration				
$k_{rw\ (Swi)}$	0	0	0	0
$k_{ro\ (Swi)}$	0.98	0.46	0.64	0.73
$k_{rw\ (Sor)}$	-	0.03	0.72	0.50
$k_{ro\ (Sor)}$	0	0	0	0

When calculating permeability by Darcy's regression the correlation coefficient was closer to 99.9%. As expected, permeability for 0.1M brine was closer to 1M brine injection.

Effective permeability for MWB_2 was reduced after wettability treatment from 3.1 D in water-wet state to 1.37 D in mixed-wet conditions, which shows a success in the wettability treatment.

Table 7. *Initial saturation state reached in every core sample after desiccation.*

(*) $m_{(Swi)}$ corresponds to mass at S_{wi}, different from $m_{(sat).}$

6.3. Wettability alteration

6.3.1. Wettability modification for MWB_1

The MWB_1 sample underwent unexpected wettability alteration results probably due to insolubility of Quilon H in n-decane. It was evidenced by a localized non-homogeneous dark coloration in the surface of the core after the treatment had been performed **Figure 10a.** This coloration covered 50 % of the sample (± 2.5 cm), gradually decreasing from the ends to the center of the core**.**

After the wettability treatment was finished, it was seen that both phases, n-decane and Quilon H, separated themselves when pouring the solution out of the piston cell and traces of Quilon solution were adhered to the bottom of the piston cell.

Additionally, remnants of Quilon solution were seen in the lines and equipment during preparation of the solution. These particles came out through the outlet flow line after a couple of hours. All these observations brought up the hypothesis that the sample underwent a precipitation process instead of an adsorption process. Chemical degradation of the solution was also suspected. These conditions may have caused pore blockage and limit the effect of Quilon solution.

Presumably, light and temperature could have also caused the Quilon H solution to react with the mineral components of the core; therefore, a stability test for the solution was conducted by preparing four samples of Quilon H solution to establish the impact of these two variables. Temperature and light conditions were systematically varied in these samples. After two

	Initial saturation state				
	MWB_1	**MWB_2**	**OWBEREA**	**OWB_3**	**Units**
$m_{(Swi)}$	226.24	226.7	223.94	227.58	g
S_{wi}	10.05	7.4	10.5	10.62	%
Soi	89.95	92.6	89.5	89.38	%

weeks of variations, visual examination of the samples did not reflect appreciable changes in color or precipitation **Figure 10b**.

Once temperature and light conditions were discarded as potential conditions affecting the properties of Quilon H, it was determined that Quilon H was not soluble in n-decane. Thus, MWB_1 was separated in 3 parts. The middle part, which was not in direct contact with Quilon H, was split and immersed in n-decane to be preserved. Following, the wettability treatment with Quilon L was performed. This chemical has the same composition but higher grade than Quilon H. Unlike the initial trial (MWB_1), the solution was stable and homogeneous, and there were no signs of separation and/or precipitation in the lines or in the piston cell. This positively indicated that Quilon L was suitable for the experiment and hence it was used for performing the wettability treatment in the MWB_2 and OWB_3 samples.

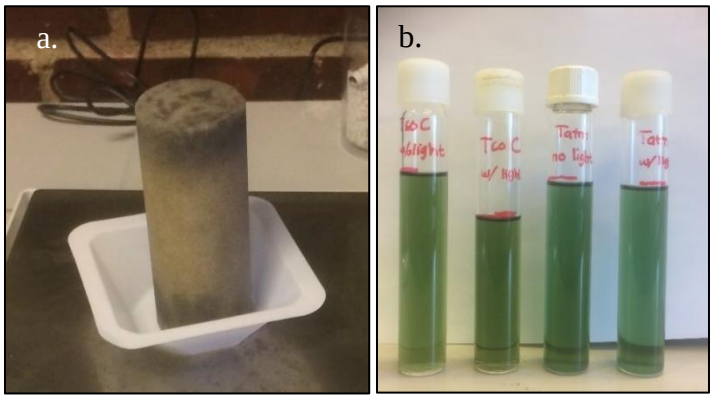

Figure 10. *a) Coloration of the surface in MWB_1 after wettability treatment using Quilon H. b) Samples used for testing Quilon H in different temperature and light conditions.*

6.3.2. Wettability modification for MWB_2

PVs of the injected Quilon solution were determined by the stabilization in pressure drop and the coloration of the effluent. This latter factor was the most important when deciding when to stop injection. According to this, 9.6 and 5.8 PVs were injected in the first and second direction respectively. The effluent was lighter during the early stages of the 1st direction, where n-decane was displaced by Quilon solution. In the 2nd direction, the effluent was darker which indicated that Quilon had been flowed through the entire core. **Figure 12** shows the variation in color during 1st and 2nd direction.

Effluent color of n-decane injection to flush out Quilon is shown in **Figure 13**. Coloration of the effluent dissipated after 3PVs had been injected. Clear coloration of the effluent after injection of 6.85 PVs of n-decane indicated the end of the process. Conditions of MWB_2 before and after wettability treatment are presented in

Figure 11.

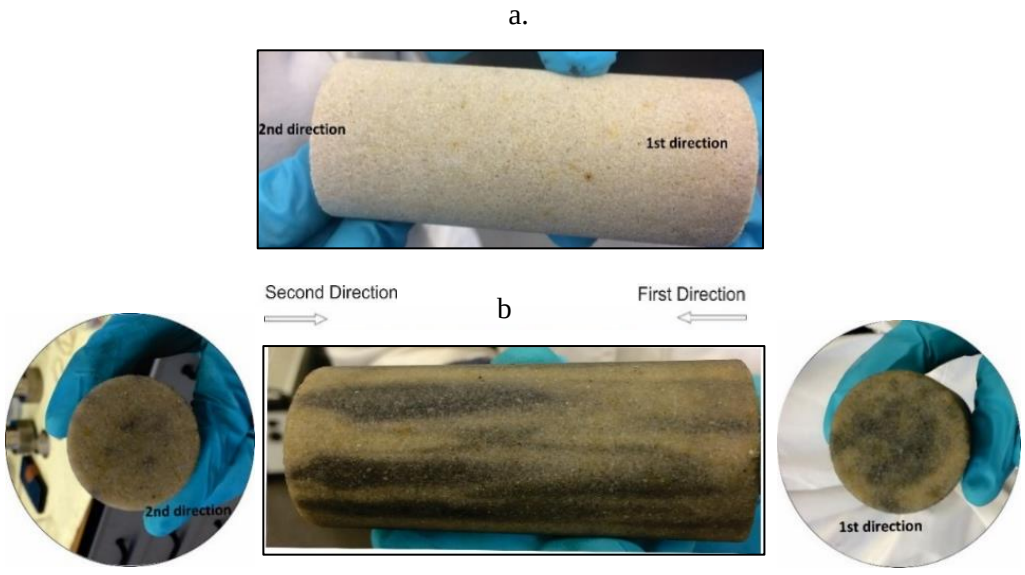

Figure 11. *Final condition of MWB_2 a) before and b) after wettability treatment with Quilon L solution (3% wt).*

Figure 12a showcases the effluent obtained from Quilon L (3% wt) during first and second direction. Effluent after injection of n-decane is shown in **Figure 13**.

a.

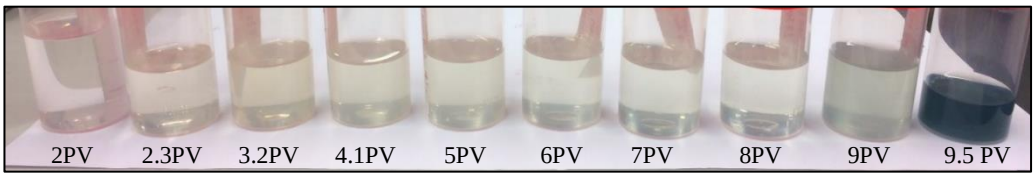

b.

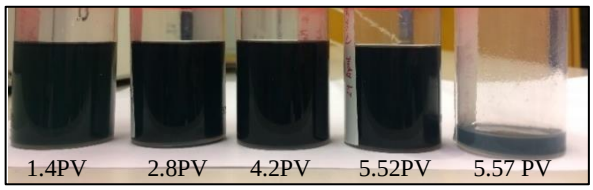

Figure 12. *Effluent of Quilon L Solution (3%wt) after injection of a) 9.6 PVs in the first direction b) 5.8 PVs in the second direction in MWB_2.*

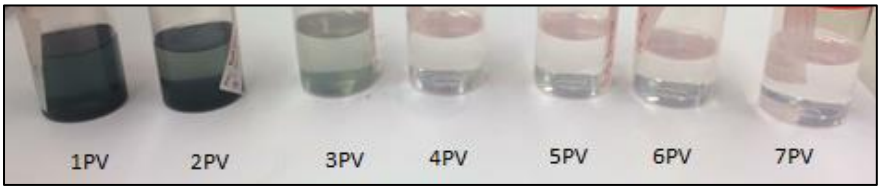

Figure 13. *Effluent of n-decane after Flush out of Quilon L in MWB_2 wettability alteration.*

Pressure drop (dP) during the three stages of injection of Quilon for MWB_2 is presented in **Figure 35**. Some spikes arose due to noise from the source pump. Refined data for dP was computed in excel as a trend line.

6.3.3. Wettability modification for OWB_3

The conditions of OWB_3 core can be examined below. This sample does not show a significant change in color after Quilon injection, but it did change after temperature aging at 95°C in the oven. Dark coloration at the bottom of the core is original from the untreated sample.

a. b. c.

Figure 14. Conditions of OWB_3 a) before, b) after wettability alteration using Quilon L solution (3% wt) and c) after temperature aging at 95° in the oven.

Pressure drop for OWB_3 had to be corrected to zero dP (0.27 mbar) since the core holder remained vertical during Quilon injection. The average pressure during Quilon injection remains at 2.8 mbar when injecting 10 PVs in both directions. Pressure drop during Quilon treatment can be examined in ***Appendix 2***, **Figure 36**.

Figure 15a and **b** show the effluent collected in both directions from injection of Quilon-L in distilled water for OBW_3. **Figure 15c** shows the position of the core holder as stated in the technique implemented by (Maini et al., 1986).

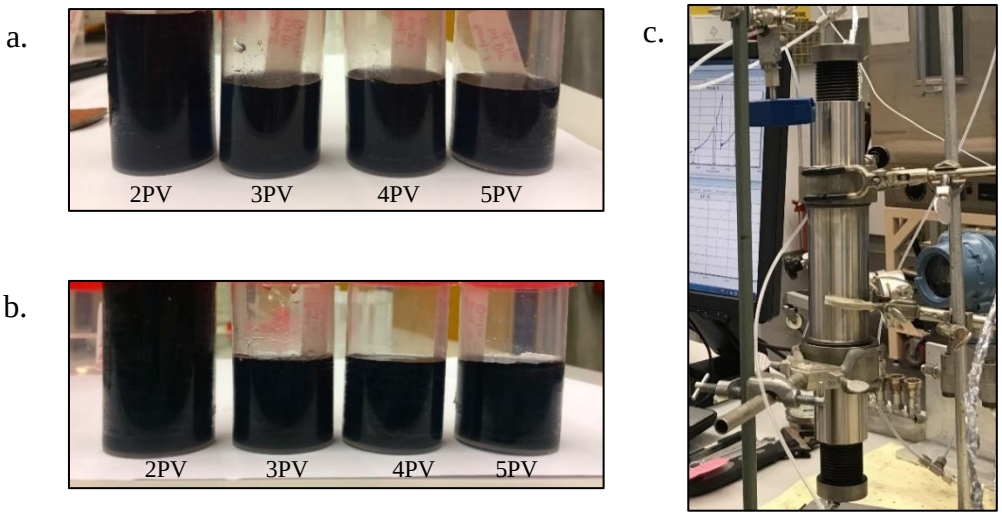

Figure 15. Effluent collected from injection of Quilon L solution (3% wt) in the a) 1st direction; b) 2nd direction; c) Vertical position of core holder for injection of Quilon L in OWB_3.

6.4. Imbibition Test

Figure 16**Figure *17*** and **Figure 17** show a cartesian and semi-log plot, respectively, for oil recovery vs time during spontaneous imbibition for the MWB_2, OWB_3, and OWBEREA samples.

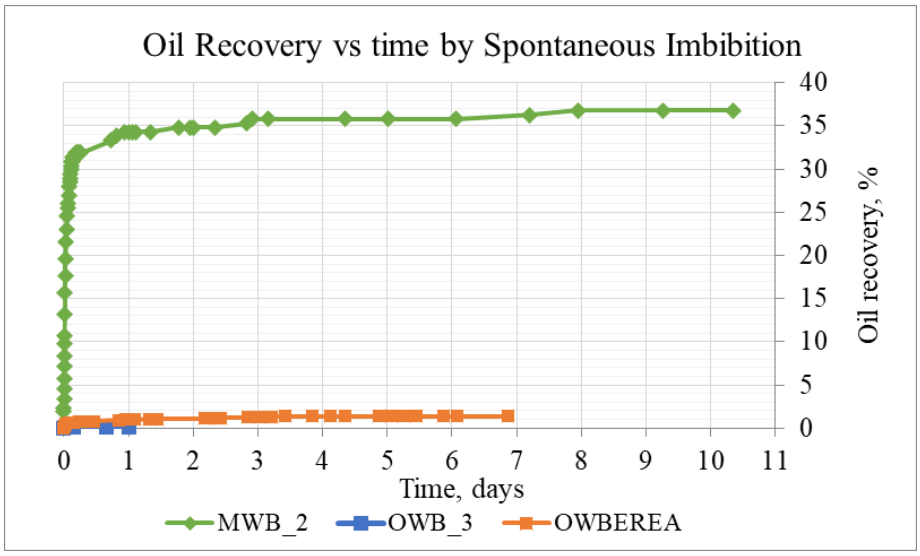

***Figure 16**. Oil Recovery vs time for MWB_2, OWB_3, OWBEREA during spontaneous Imbibition*

The two oil-wet samples (OWBEREA and OWB_3) showed insignificant oil recovery during the process. For OWB_3, 0.01 ml of oil was produced after 17 days with water saturation increasing from 10.62% to 10.67% (**Table 8**). For OWBEREA, 0.26 ml of oil were collected after 7 days, and water saturation went from 10.05% to 12% (**Table 8**). Both samples exhibited oil recovery lower than 2%. This low recovery was a clear indication that the wettability alteration (from strong water-wet towards oil-wet state) performed during this work was successful as significant production was no expected under oil-wet conditions (c.f. Anderson, 1987).

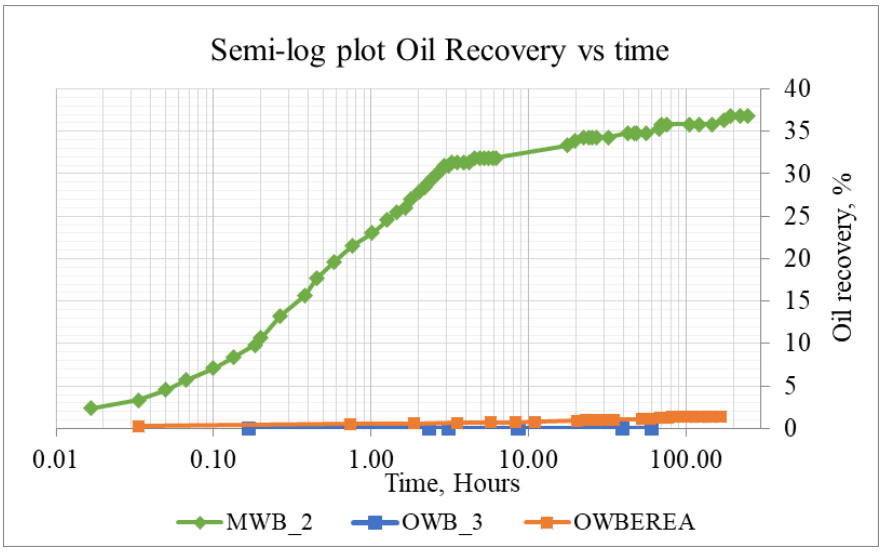

Figure 17. Semi-log plot of oil recovery vs time for MWB_2, OWB_3, OWBEREA during Spontaneous Imbibition.

On the other hand, oil production in MWB_2 increased a lot faster than oil-wet cores (OWB_3 and OWBEREA). Most of the oil was effectively produced at the beginning. 7.4 ml of oil were produced during the first 7 days. After 10 days of imbibition, water saturation increased from 7.4% to 41.5% in this core (**Table 8**). These results were expected due to the mixed-wetting state that was established in this core.

In the light of these observations, recovery in the mixed-wet core (MWB_2) was significantly higher compared to oil-wet cores (OWB_3 and OWBEREA) due to wetting conditions. In the MWB_2, the flow of the oil phase is inferred to have been easier since larger pores are strongly oil-wetted, whereas smaller pore surfaces remain preferentially water-wet (Salathiel, 1973). In the oil-wet cores, spontaneous oil production was lower since capillary forces tend to retain the oil phase in the pores. Likewise, under oil-wet conditions, water forms continuous channels through the center pushing oil partially out (Anderson, 1987). However, under either oil or mixed-wet conditions, the oil remaining in the core can only be removed by applying external forces during forced imbibition tests.

In a Pc curve for spontaneous imbibition tests, it could be predicted that water saturation (S_w) for oil-wet samples (OWB_3 and OWBEREA) will be placed to the left of mixed-wet samples (MWB_2). Hence, this is indicative of low imbibition of water in the cores.

6.5. Forced imbibition

Figure 18 and **Figure 19** depict pressure drop and produced oil vs PV for OWB_3 during forced imbibition test. Each increment of rate was dictated by the stabilization of both parameters. The lowest flow rate was 0.0092 ml/min and the largest was 7.5 ml/min, which was the maximum rate provided by the pump.

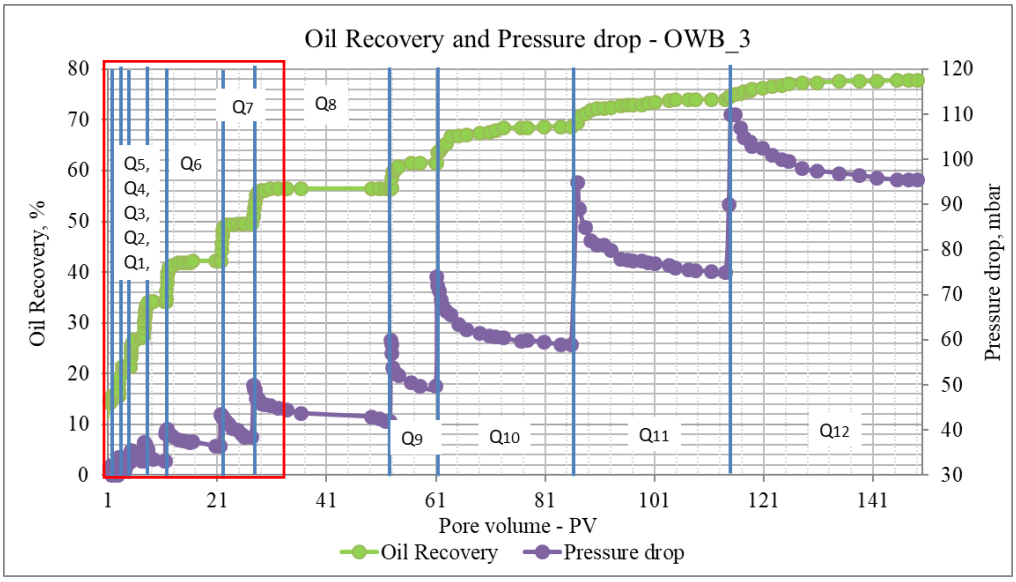

Figure 18. Profile of oil production and pressure drop vs PV for OWB_3 accounting for End Effects during waterflooding of higher flow rates. The red square outlines the lowest values presented in **Figure 19**.

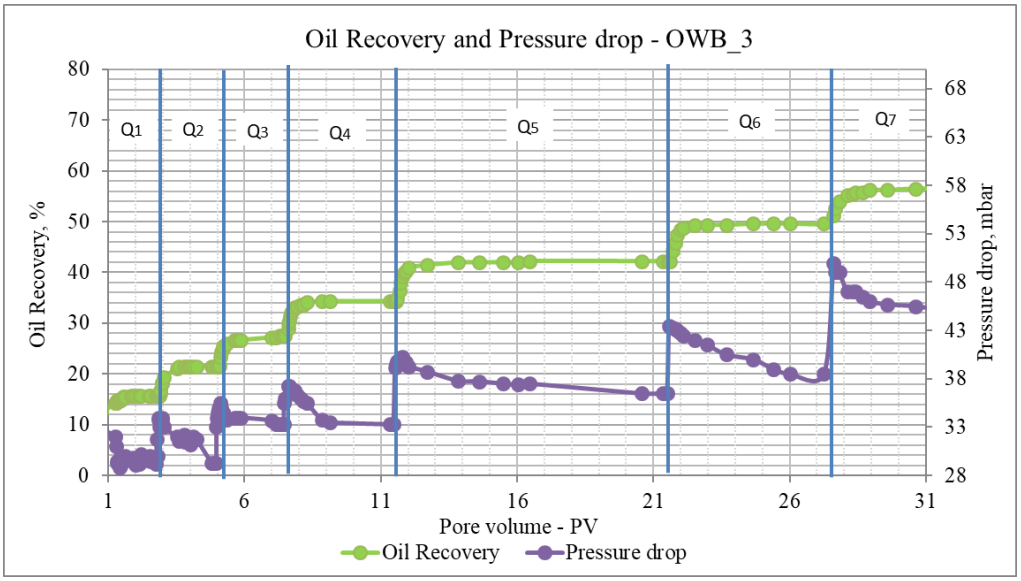

Figure 19. Blow up of the lowest flow rates presented in **Figure 18**.

End Effects for OWB_3 are presented in **Figure 18** and **Figure 19**. A clear indication of the presence of capillary End Effects was additional oil recovered after an increment in the flow rate (and hence the pressure differential). Significant oil production occurred when increasing the rate during the initial stages. However, CEE were seen to be drastically reduced during increments at higher rates, mainly above Q10 (153.6 PV/day). These observations give way to conclude that this a rate-dependent process.

These outcomes are in agreement with theory and allows us to conclude that oil was retained at the outlet end of the core by the action of capillary forces as a result of CEE (Geffen et al., 1951; Richardson et al., 1952). This should not be ruled out, however, that this decrease in oil production could have also resulted from the normal decrease of oil saturation throughout the core towards Sor.

The obtained results positively confirm that the experimental design and its implementation was successfully carried out around CEE in unsteady state core-flooding, supporting theoretical explanations by Gupta and Maloney (2016), Andersen (2017), Qadeer (1988); Heaviside and Black (1983); Hadley and Handy (1956); Osoba et al. (1951).

.

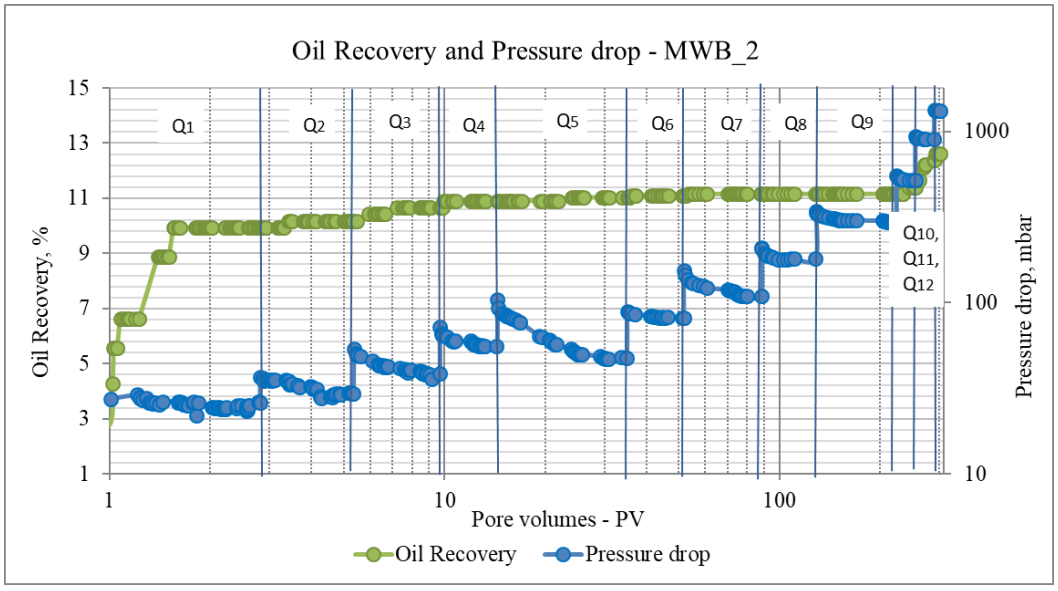

Figure 20. Log-log Profile of oil production and pressure drop vs PV accounting for End Effects in MWB_2.

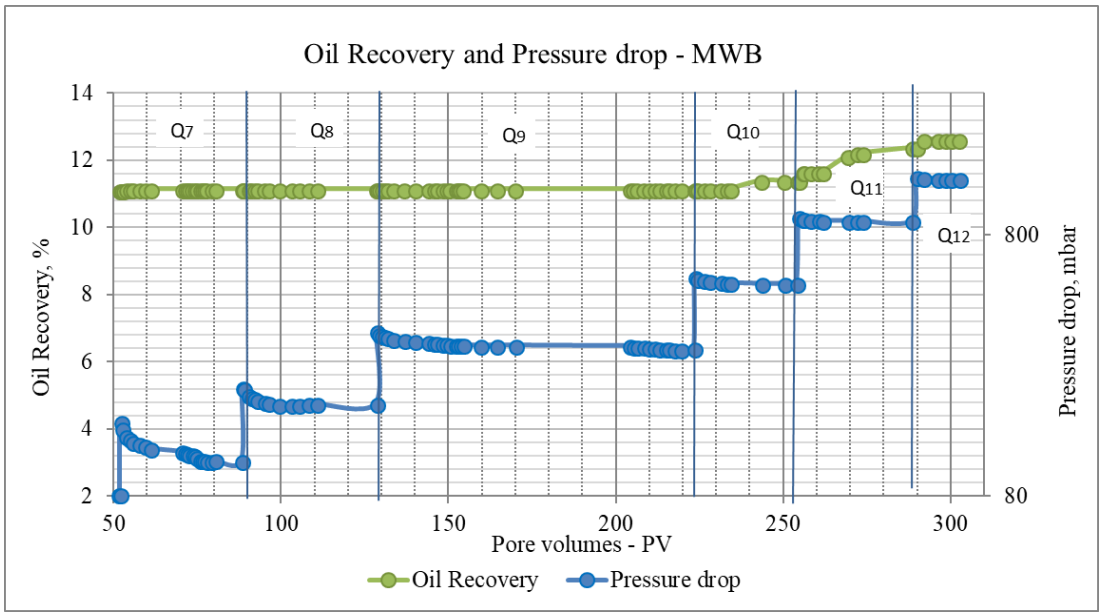

Figure 21. Profile of oil production and pressure drop for MWB _2 accounting for End Effects during waterflooding at higher flow rates.

Figure 20 illustrates the oil recovery and pressure drop profiles vs injected PV for MWB_2. In **Figure 21** oil production is zoomed in for largest flow rates.

Unlike OWB_3, no significant oil recovery increment was seen in MWB_2 after changing the rates at early stages (**Figure 20)**. Oil was produced substantially during the last rates, 307.2 PV/day (Q11) and 490.46 PV/day (Q12). Low recovery at early stages was likely due to reduced oil saturation in the sample since most of the oil was produced by spontaneous imbibition. Additionally, some oil unexpectedly flowed towards the pressure line during the initial rate (0.0061ml/min). That oil was allocated to this corresponding rate, but it is likely that some oil could have been lost somewhere else in the set-up. Despite of this unpredicted behavior, oil recovery of MWB_2 seemed to be still a rate-dependent process.

High recovery at relatively high rates can be explained by the fact that oil obtained at the effluent was not necessarily squeezed from the core itself. It could have also been oil accumulated in the pipelines. Observations from both tests consistently show deviation from standard Buckley-Leverett theory (Buckley and Leverett, 1942), which predicts no rate dependence production when Pc = 0.

Table 8 shows the water saturations obtained at the end of Spontaneous and Forced imbibition tests.

Table 8. *Table with saturation and oil recovery for each core after forced and spontaneous Imbibition.*

	OWBEREA	***MWB_2***	***OWB_3***	***Remark***
PV	20.840	22.020	21.980	
S_{wi}	0.105	0.074	0.1062	S_{wi} *after dessication*
(S_{wi}, SI)	0.120	0.415	0.1067	S_{wi} *after Spontaneous Imbibiton*
$(S_{wi}, FI)_{vol}$	0.360 *	0.532	0.803	S_{wi} *after Forced Imbibiton measured by volume*
$(S_{wi}, FI)_{wt}$	-	0.588	0.819	S_{wi} *after Forced Imbibiton measured by weight*
OIIP	18.652	20.391	19.646	

(*) S_{wi} *after Spontaneous Imbibiton* for OWBEREA at the end of the experiment was 66.5%. However, the S_{wi} presented (36%) is the one reported at the moment of the high pressure event which did not allow to finish the experiment in the suitable conditions.

6.6. Simulation results

Simulation results for OWB_3 will be discussed in this section. History match for MWB_2 could not be performed accurately by Sendra since most of the oil was produced by Spontaneous Imbibition. Saturation range for capillary pressure during forced imbibition was limited between 41.46% and 53.15%.

6.6.1. Relative Permeability and Capillary pressure Curves

In the relative permeability curve for OWB_3 obtained in the simulation (**Figure 22a)**, it is seen that oil relative permeability (K_{ro}) drops rapidly, while water relative permeability (K_{rw}) rises rapidly. It occurred because of the oil-wetting state in the sample as water flows through the largest flow channels first in these conditions.

a. b.

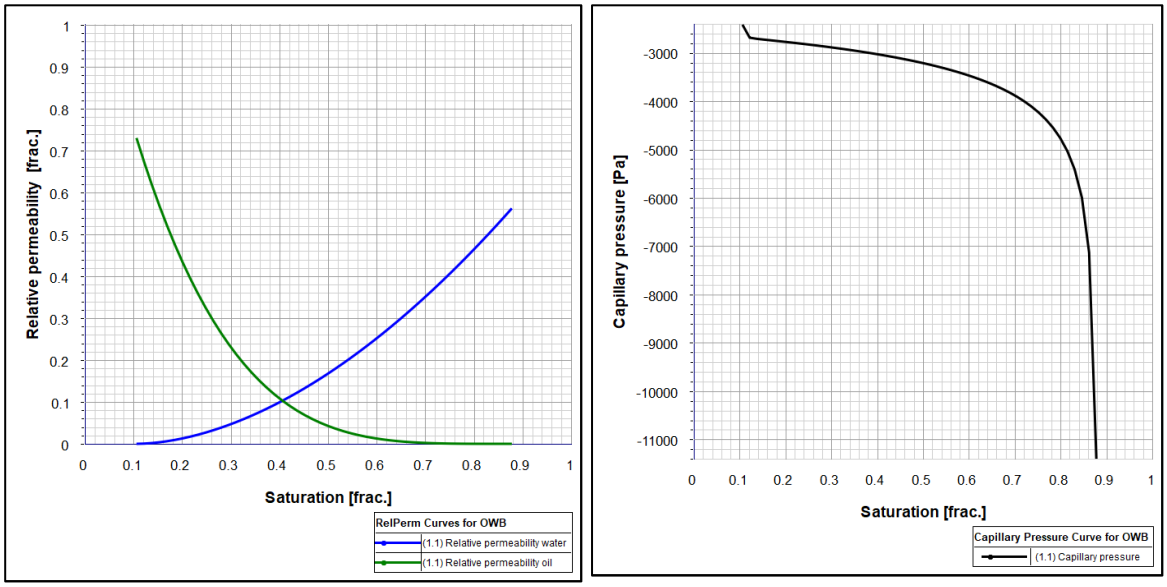

Figure 22*. Simulated a) Relative permeability and b) Capillary pressure for OWB_3.*

The relative permeability end points were determined during the Forced imbibition experiment **(Table 9b)**. However, Sor and k_{rw} (S_{or}) were estimated by the simulator in order to allow the software to find the best fit between the experimental and simulated data.

Experimental values for $k_{rw(Sor)}$ and S_{or} were found to be 0.727 and 0.197 respectively, compared to values of 0.562 and 0.122 (**Table 9**) estimated by the simulator. This procedure did not necessarily show that $k_{rw(Sor)}$ and S_{or} were accurately determined, but the shape of the relative permeability curve was more flexible; hence, it was possible to reconcile the experimental and calculated data as seen in **Figure 23**.

Table 9*. a) Parameters obtained from simulation and b) endpoints from laboratory experiment as input variables for OWB_3.*

a) Parameters obtained from Sendra for OWB_3

Co	ao	Cw	aw	Nw	No	$k_{rw(Sor)}$	S_{or}
2599.68	0.251	0.0038	1.999	1.798	3.977	0.562	0.122

b) Input endpoints from laboratory experiment for OWB_3

S_{wi}	$k_{rw(Sor)}$	$k_{ro(Swi)}$	S_{or}
0.1062	0.727	0.73	0.1973

Water saturation is increased inside the core either by spontaneous or forced Imbibition. In a capillary pressure curve, positive values represent oil is released by spontaneous imbibition, whereas values below zero represent oil recovered by forced Imbibition.

The capability of Sendra software, however, is limited to forced imbibition experiments, hence, positive capillary pressure was not modelled in this study. It should also be pointed out that production stabilization by spontaneous imbibition is characterized by zero capillary pressure on the curve. At that point, advective forces in the core are strong enough to equilibrate capillary forces; therefore, no more spontaneous imbibition takes place since all the water-wet pores in the core has been filled up with oil and the surface energy reduced to its minimum. Capillary pressure curve indicates that an applied differential pressure will be required for water to enter to the core to displace the oil. Capillary forces can be measured indirectly as the response of the amount in oil production, whereas production stabilization is obtained as a response of rate.

The capillary pressure curve in this study was constrained using Skjaeveland parameters in the Skjaeveland correlation (c.f. Skjaeveland et. al., 1998) (**Table 2a**). Oil that was trapped by capillary forces at Pc=0 was later pushed out by means of increasing rates. This produced oil is represented by negative values in the capillary pressure curve (**Figure 22b**).

6.6.2. History Matching

The overview for the history match of pressure drop and oil production experimental data is shown in **Figure 23**. Both experimental and simulated curves fit properly when estimating $k_{rw(Sor)}$ and S_{or} end points.

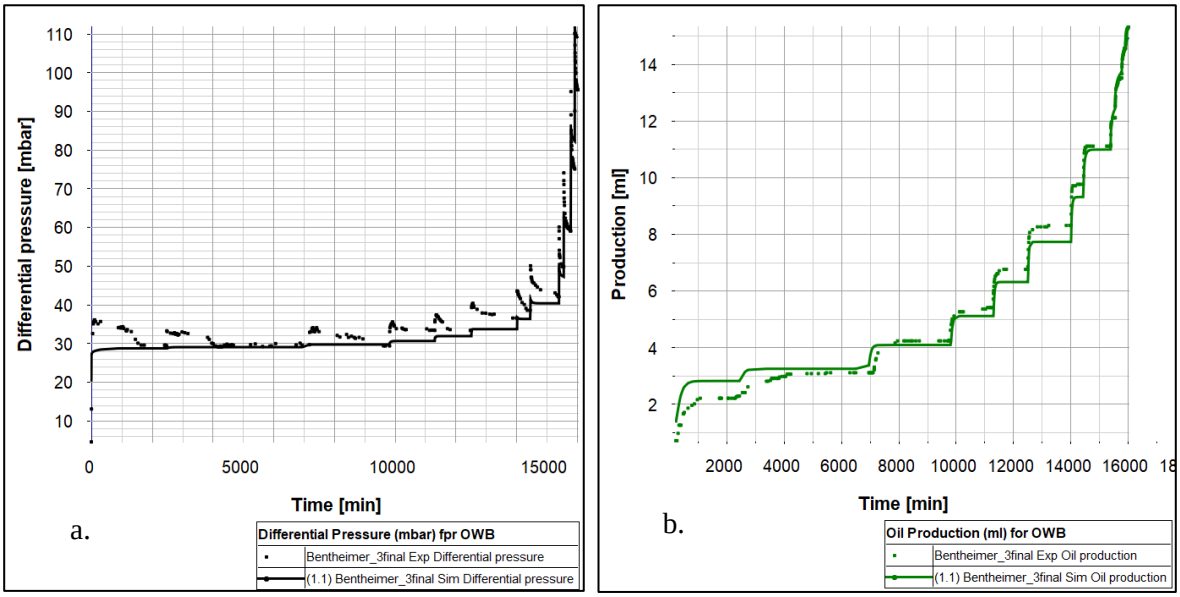

***Figure 23**. History Matching of a) differential pressure and b) oil production for OWB_3.*

6.6.3. Saturation Profile with varying Flow Rate

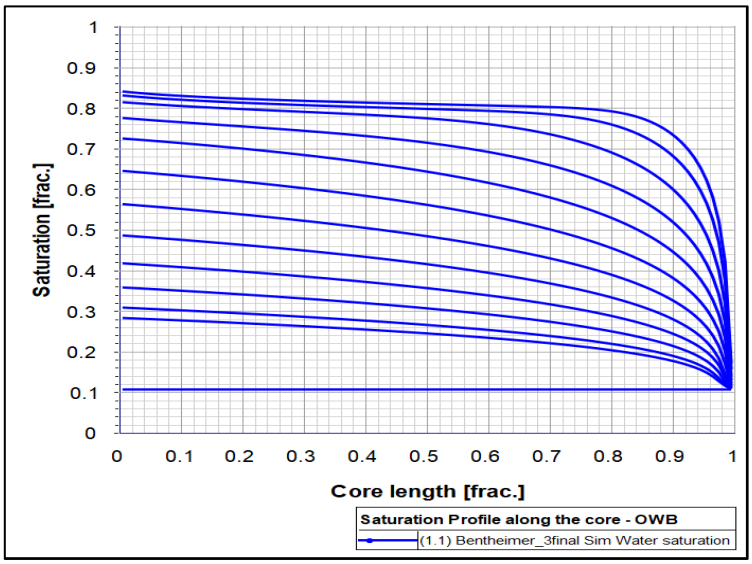

***Figure 24.** Saturation profile vs length for OWB_3*

The capillary End Effects are reflected through saturation profile for OWB_3 shown in

Figure 24. Each line corresponds to the saturation profile at each specific rate. High oil saturation levels show the impact of low flow rates injected into the core during the experiment. Thus, at high flow rates, oil saturation in the core is reduced, indicating that the

advective forces (given by the rate) are strong enough to sweep most of the oil in the oil-wet core. It inherently brought about higher oil displacement followed by higher production as seen in **Figure 24**. The saturation at the outlet at all given rates converged to the initial water saturation as an effect of the capillary end effect.

6.6.1. Saturation Profile with varying Water Viscosity

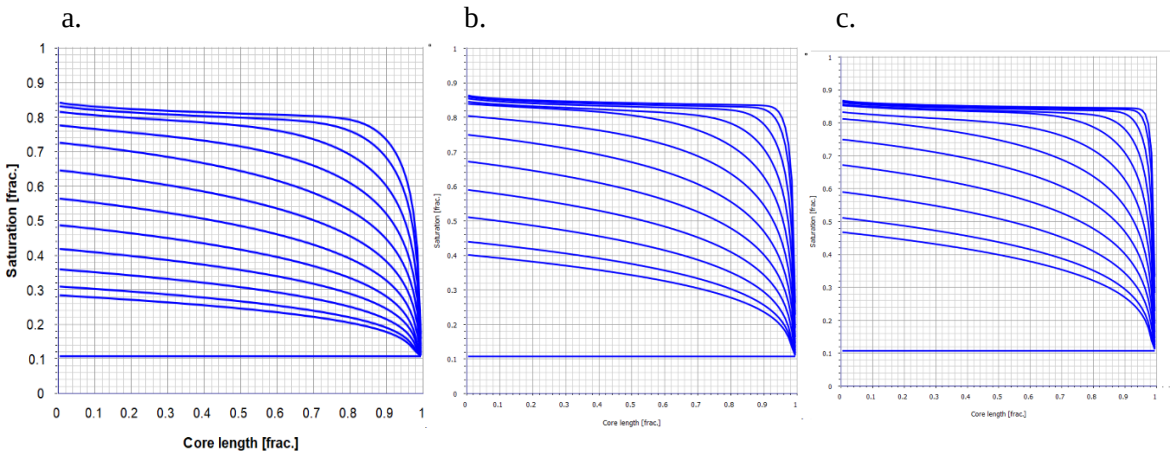

Figure 25. Water Viscosity sensitivity a) μ b) 5 times μ c) 10 times μ.

A sensitivity analysis for water viscosity was performed in order to assess the impact of this parameter on the end effects (Figure 25). Water viscosity was increased 5 and 10 times in figure 25a and b, respectively. It can be seen that the shape of the curve at the upper right corner varied from a smooth curvature in figure 25a to a rather sharp/angular curvature in figure 25b and c. This variation in the curvature indicates that CEE tend to be minimize as oil saturation in the core is approaching the Sor. Hence, the saturation profile tends to be closer to the residual oil saturation at the highest rates. It is also observed that higher water viscosity causes higher volume of oil produced at the lowest rates.

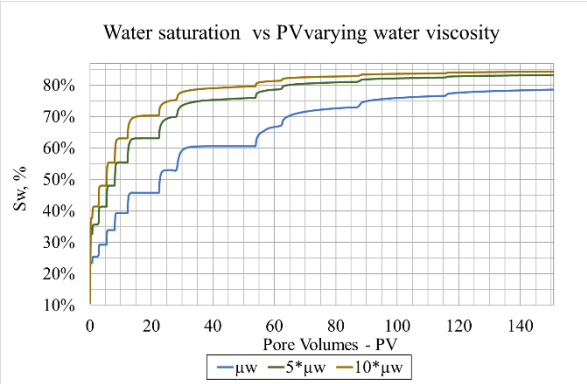

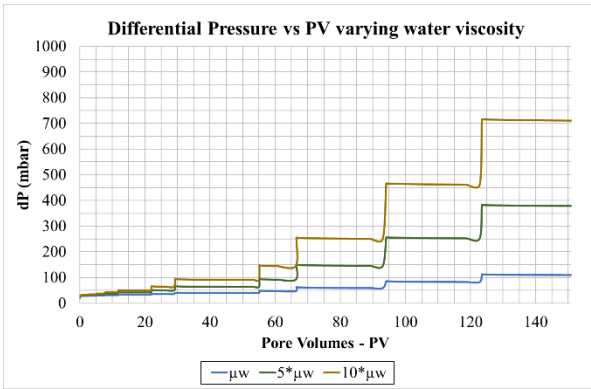

Figure 26.a) Water saturation profile and b) differential pressure for OWB_3 for sensitivity of water viscosity.

By increasing the water viscosity, oil production is also higher. It occurs because higher viscosity removes the fingered displacement effect and, hence, the displacement of oil through the core will be more homogenous due to an enhanced displacement front (Mohanty and Miller, 1991). Therefore, in **Figure 26a,** Sw increases with increased water viscosity. It should be highlighted, however, that the most significance difference in Sw is seen between 0 water viscosity increment (blue line) and 5 water viscosity increment (dark green line). **Figure 26b** shows that as more oil is push out of the core, the differential pressure is also increased.

6.6.2. Saturation Profile with NO End Effects

On the other hand, this work presents simulation results for oil production and saturation profile when capillary End Effects were minimized. To minimize capillary End Effects, it is often recommended to use higher flow rates or longer core samples (Hinkley and Davis, 1986; Qadeer et.al., 1988). In this case, enlarging the length of the core to run the simulation was not possible since experimental data accordingly was not available. Then, to obtain the saturation profile with no End Effects was necessary to use high flow rate and Pc equal to zero in order to avoid oil trapping in the core due to capillary forces.

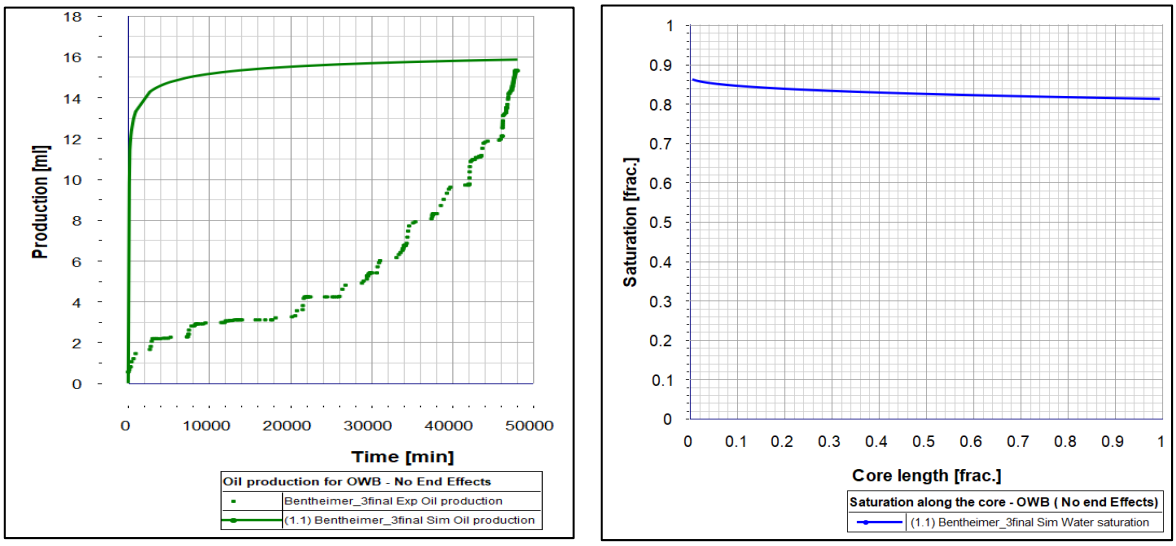

Figure 27 a) Oil production and b) Saturation profile for OWB_3 with no CEE.

Oil production with no Capillary End Effects showed oil being produced at once followed by a lasting period of gradual increase until reaching stabilizing conditions (solid line in **Figure 27a)**. It contrasts with a generally ascending, step by step (dotted line in **Figure 27a)** oil production trend when accounting for CEE.

The saturation profile in this case was constant until reaching the outlet end of the core (**Figure 27b**). Then, most of the oil saturation was drained out of the core by applying a relatively high constant flow rate.

7. Conclusions and Future Work

End effects are frequently experienced in laboratory set-ups, but are deliberately avoided in the experiments for determination of relative permeability. In this study, RelPerm and Pc curves accounting for Capillary End Effects (CEE) were obtained. A simulation tool was used to perform the history matching of experimental pressure drop and oil production obtained from an unsteady-state lab experiment. A general procedure to conduct floodings in oil-wet samples was developed.

The results of this work lead to the following conclusions:

- End effects were stronger during low rates since little oil was produced. It demonstrates that oil production is in fact a rate dependent-process during waterflooding when accounting for CEE. This observation is in disagreement with Buckley-Leveret theory (Buckley & Leverett, 1942), which claims the non-dependency oil production with rate.
- Oil production under no Capillary End Effects occurred mostly at once during the early stages of production, whereas it occurred in a step-like manner when accounting for Capillary End Effects. It highlights the importance of taking into account CEE to obtain more realistic Relperm and Pc for prediction of fluid flow through porous medium.
- After several trials, Quilon L proved to be more effective than Quilon H when inflicting wettability modification.
- It was seen that higher water viscosity reduces Capillarity End effects, and increases oil production at the lowest rates.
- It was checked the success of the wettability alteration in the core plugs by the spontaneous imbibition method. Oil-wet samples were not allowed to imbibe too much water which indicates that capillary forces tend to retain the oil phase in the pores.
- The obtained results indicate that the experimental design was successfully carried out for unsteady state core-flooding. Likewise, the results are consistent with theoretical explanations by Gupta and Maloney (2016); Andersen (2017); Qadeer (1988); Heaviside and Black (1983); Hadley and Handy (1956); Osoba et al. (1951).

- As extended periods of time had to be allowed for reaching stabilized differential pressure and oil production at lower rates, it is recommended looking for an alternative approach to estimate a steady-state tendency through early stages of stabilization. Besides, it is important to determine controlling factors to reach stable conditions for pressure drop and oil production during waterflooding when accounting for CEE.

- It would be useful to conduct a similar study to constrain Pc and RelPerm curves for core samples of the same nature but different wettability states, and then compare the results from different wetting conditions.

- For future experimental work, it would be advantageous to ensure that pipelines are cleaned properly after being in contact with a chemical for wettability alteration. That is important because it may cause erroneous measurements in the oil production. Having short outlet pipelines would also reduce the error in the measurements of oil caused by the dead volume.

Appendix

Appendix 1. Permeability Tests

Permeability tests for first Bentheimer, Berea, OWB and MWB are shown in this section. Every chart displays the flow rate in ml/min and pressure drop in mbar in the y-axis vs the number of injected pore volumes in the x-axis. A decrease in pressure drop in every sample occurred when performing 0.1 M brine injection at 0.5 ml/min, right after 1M brine injection.

Appendix 1.1. Permeability tests for MWB_1

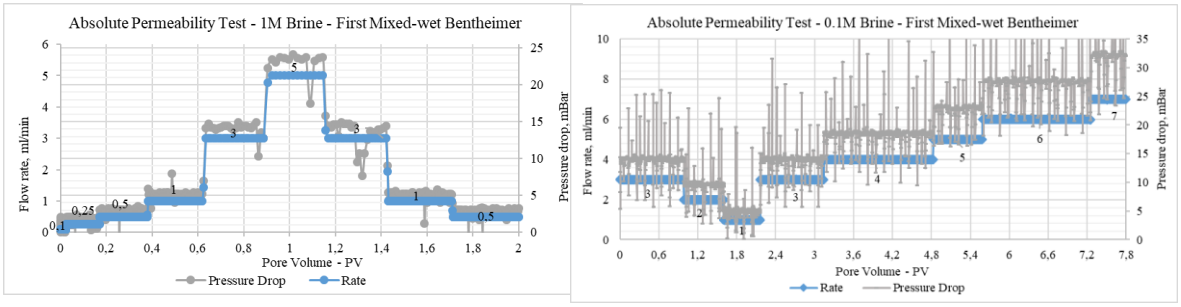

Figure 28. Illustration of pressure drop and rate vs time during the relative permeability test for MWB_1 when flowing a) 1M brine and 2) 0.1 molar brine through the core.

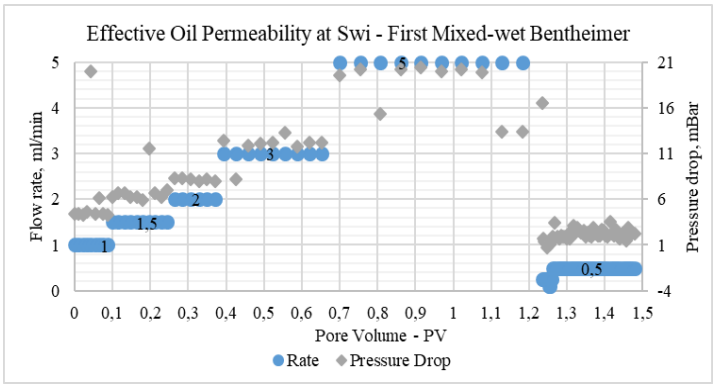

Figure 29. Illustration of ramping rates and pressure drop for calculating effective permeability of oil at S_{wi} in First mixed Bentheimer at water-wet conditions.

Appendix 1.2. Permeability Tests for OWBEREA.

Permeability tests after wettability change, and imbibition tests were performed for an already treated oil-wet Berea sample. However, during forced imbibition, confining pressure was loosened and oil was released around the core. This condition prevented this core to be used for analysis, nevertheless this core is used for testing and supporting calculations in MWB and OWB.

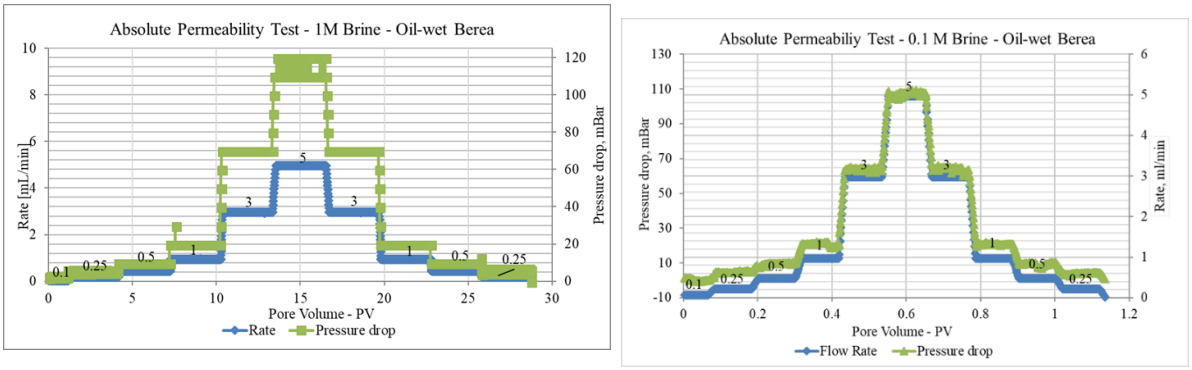

Figure 30. Illustration of pressure drop and Rate vs time during relative permeability test for OWBEREA by injecting a) 1M brine, b) 0.1 M brine.

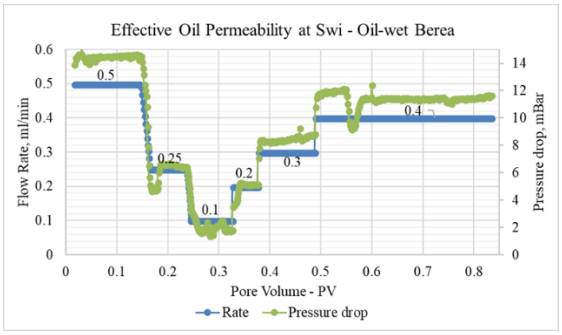

Figure 31. Illustration of ramp up rate and pressure drop for calculating Absolute permeability of oil at S_{wi}.

Appendix 1.3. Permeability tests for MWB_2

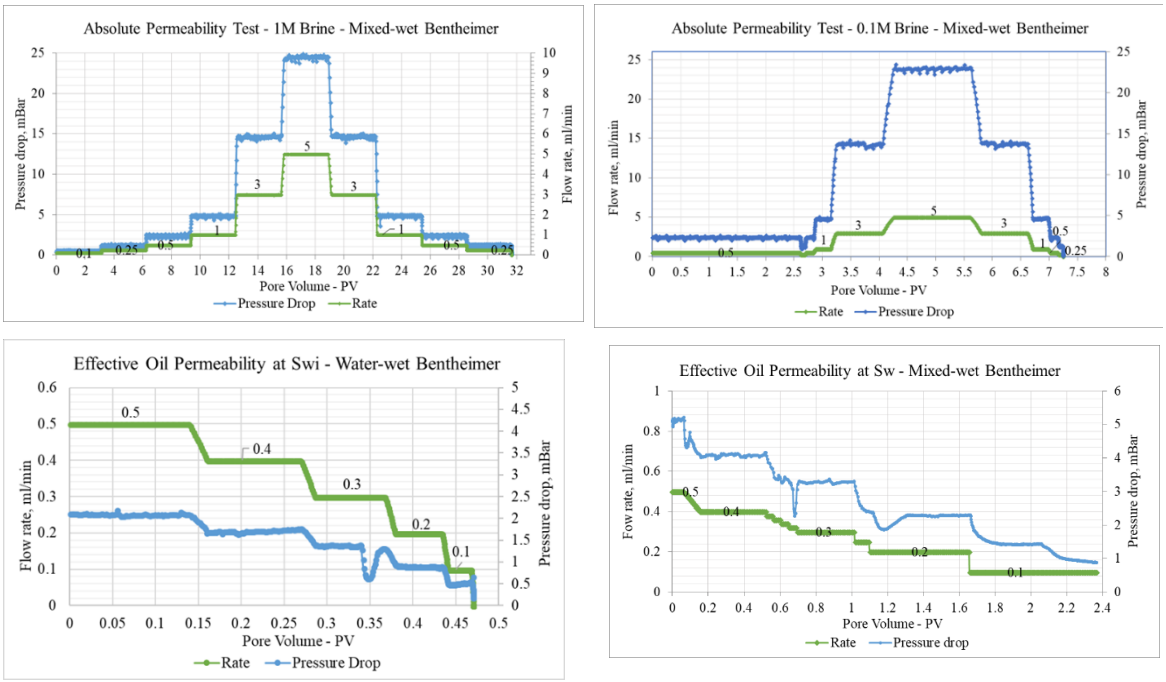

Figure 32. Illustration of pressure drop and Rate vs time during relative permeability test for MWB_2 by injecting a) 1M brine, b) 0.1 M brine, c) n-decane at water-wet conditions and d) n-decane at mixed-wet conditions during flush out of Quilon. Rate was ramped up and down through the core.

Appendix 1.4. Permeability tests for OWB_3

Due to unavailability of a high-quality pump able to record data, 1M permeability test in OWB_3, could not be recorded. Instead, results are summarized in the permeability calculation section.

Figure 33. Illustration of Pressure drop and rate profiles performed in OWB_3 to compute

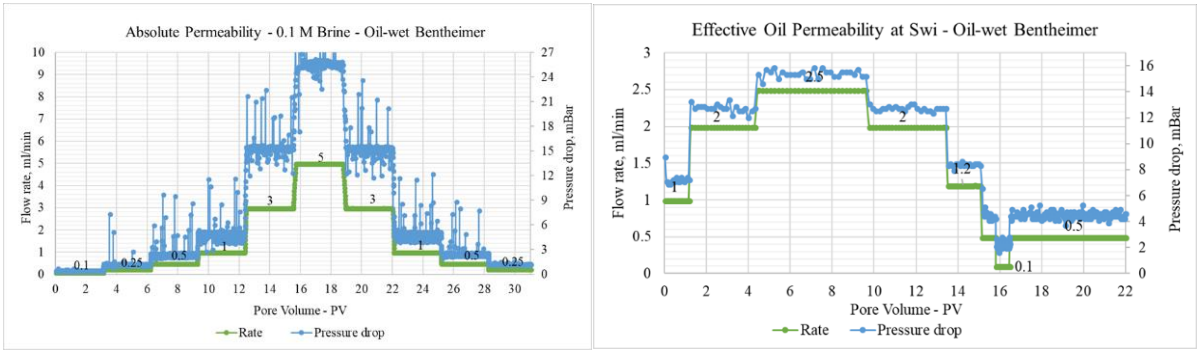

a) absolute relative permeability by using 0.1 Molar brine and b) effective permeability of oil at S_{wi} by injecting n-decane.

Appendix 2. Pressure drop during wettability treatment

In **Figure 34** pressure drop of Quilon injection of MWB_1 towards mixed-wetting can be examined. During injection in first and second direction, pressure drop rises up, and it increases even steeply during second direction. However, during n-decane flush out pressure drop become stable.

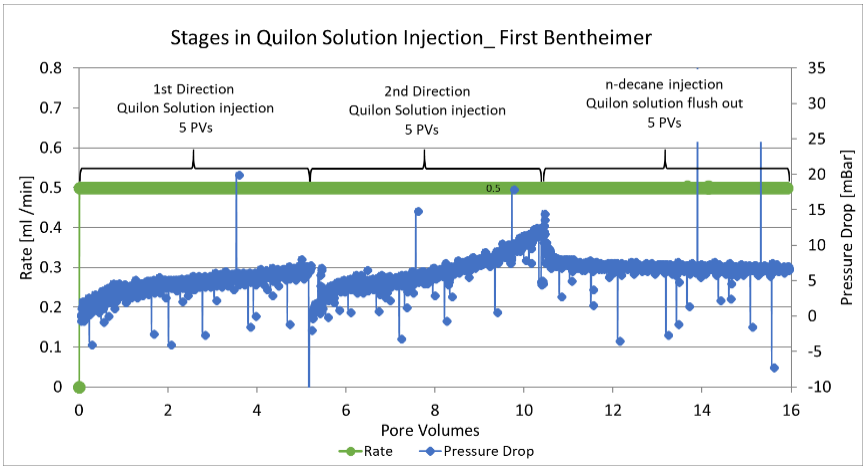

Figure 34. Stages in wettability alteration of MWB_1. It is shown injection of Quilon L in 1st and 2nd directions, as well as flush out of Quilon Solution. Five pore volumes were injected in each stage.

Pressure drop caused by injection of Quilon L in **MWB_2** is presented in **Figure 35**. Blue line represents pressure drop raw data, and the black line corresponds to smooth data.

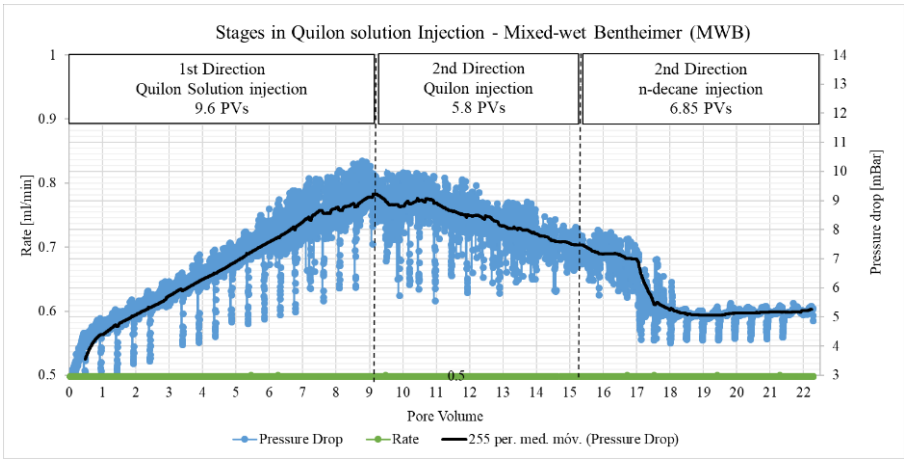

Figure 35. Pressure drop stages during wettability treatment for MWB_2 showing 1st and 2nd direction of Quilon injection and n-decane flush out. 22.5 Pore volumes were injected through the core.

A slight decrease in pressure drop at the beginning of the second direction is due to alteration of the position of the core holder while reversing the direction. The main difference with Quilon injection in First Bentheimer (**Figure 34**) is the decreasing trend during second direction. Higher values of pressure drop were found in MWB along the treatment.

Figure 36 shows the pressure drop during Quilon injection in **OWB_3**. 5Pvs injected in each direction. The green line corresponds to raw data, which shows noise from the pump. The black line corresponds to the refined Pressure drop data.

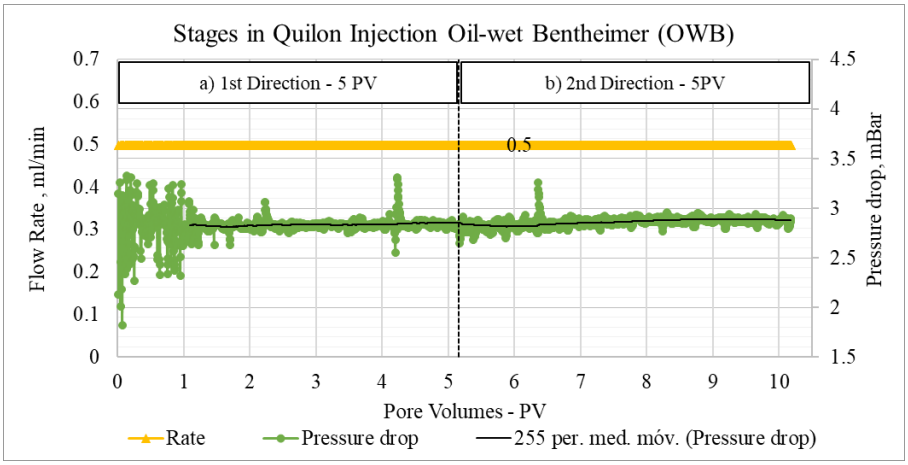

Figure 36. Stages during Quilon injection in OWB_3. a) 1st direction and b) 2nd direction. 10 PVs injected through both directions.

References

Abdallah, W., Buckley J., Carnegie, A., Edwards, J., Herold, B., Herold, E., Graue, A., Habashy, T., Seleznev, N., Signer, C., Hussain, H., Montaron, B., Ziauddin, M. (2007). Fundamentals of wettability. Schulumberger Wettability Workshop, Bahrain.

Abeysinghe, K. P., Fjelde, I., and Lohne, A. (2012, January 1). Dependency of Remaining Oil Saturation on Wettability and Capillary Number. Society of Petroleum Engineers.

Andersen, P. Ø., Standnes, D.C, Skjæveland, S.M. (2017). Waterflooding oil-saturated core samples - Analytical solutions for steady-state capillary End Effects and correction of residual saturation. Journal of Petroleum Science and Engineering, v. 157, p 364-379.

Anderson, W. G. (1986). Wettability Literature Survey- Part 1: Rock/Oil/Brine Interactions and the Effects of Core Handling on Wettability. Society of Petroleum Engineers.

Anderson, W. G. (1986). Wettability Literature Survey- Part 2: Wettability Measurement. Society of Petroleum Engineers.

Anderson, W. G. (1986). Wettability Literature Survey-Part 3: The Effects of Wettability on the Electrical Properties of Porous. Society of Petroleum Engineers.

Anderson, W. G. (1987). Wettability Literature Survey- Part 4: Effects of Wettability on Capillary Pressure. Society of Petroleum Engineers.

Anderson, W. G. (1987). Wettability Literature Survey Part 5: The Effects of Wettability on Relative Permeability. Society of Petroleum Engineers.

Askarinezhad, R., Hatzignatiou, D. G., and Stavland, A. (2017). Disproportionate Permeability Reduction of Water-Soluble Silicate Gelants: Importance of Formation Wettability. Society of Petroleum Engineers.

Brown, R. J. S. and Fatt, I. (1956). Measurements Of Fractional Wettability Of Oil Fields' Rocks By The Nuclear Magnetic Relaxation Method. Fall Meeting of the Petroleum Branch of AIME. Los Angeles, California, Society of Petroleum Engineers.

Civan, F. and Donaldson, E. C. (1989). Relative Permeability From Unsteady-State Displacements With Capillary Pressure Included. Society of Petroleum Engineers.

Corey, A.T. (1954). The Interrelation Between Gas and Oil Relative Permeabilities. Producers Monthly, v. 19, no. 1, p. 38-41.

Donaldson, E., & Alam, W. (2008). Wettability. Houston, Texas: Gulf Publishing Company.

Geffen, T. M., Owens, W. W., Parrish, D. R., and Morse, R. A. (1951). Experimental Investigation of Factors Affecting Laboratory Relative Permeability Measurements. Society of Petroleum Engineers.

Glover, P. (2000). Petrophysics. University of Aberdeen. Department of Geology and Petroleum Geology, Aberdeen, United Kingdom.

Glover, P. (2001). Formation Evaluation (Book)University of Aberdeen. Department of Geology and Petroleum Geology, Aberdeen, United Kingdom.

Gupta, R., and Maloney, D. R. (2016). Intercept Method--A Novel Technique To Correct Steady-State Relative Permeability Data for Capillary End Effects. Society of Petroleum Engineers.

Hadley, G. F. and Handy, L. L. (1956). A Theoretical and Experimental Study of the Steady State Capillary End Effect. Fall Meeting of the Petroleum Branch of AIME, Los Angeles, California. Society of Petroleum Engineers.

Heaviside, J. and Black, C. J. J. (1983). Fundamentals of Relative Permeability: Experimental and Theoretical Considerations. SPE Annual Technical Conference and Exhibition, San Francisco, California. Society of Petroleum Engineers.

Hinkley, R. E. and Davis, L. A. (1986). Capillary Pressure Discontinuities and End Effects in Homogeneous Composite Cores: Effect of Flow Rate and Wettability. SPE Annual Technical Conference and Exhibition, New Orleans, Louisiana. Society of Petroleum Engineers.

Honarpour, M.M., Koederitz, L., Harvey, A.H. (1986). Relative permeability of petroleum reservoirs, CRC Press.

Honarpour, M.M and Mahmood, S. M. (1988). Relative-Permeability Measurements: An Overview. Society of Petroleum Engineers.

Huang, D. D. and Honarpour, M. M. (1998). Capillary End Effects in coreflood calculations. Journal of Petroleum Science and Engineering, v. 19, no 1, p. 103-117.

Hwang, S. I., Lee K.P, Lee, D.S., and Powers S.E. (2006). Effects of fractional wettability on capillary pressure–saturation–relative permeability relations of two-fluid systems. Advances in Water Resources, v. 29, no 2, p. 212-226.

Kestin, J., Khalifa, E., Correia, R. (1981). Tables of the Dynamic and Kinematic Viscosity of Aqueous NaCl Solutions in the temperature Range 20-150 °C and the pressure range 0.1 – 3MPa. Division of Engineering, Brown University, Providence.

Kyte, J.R. and Rapoport, L.A., (1958). Linear waterflood behaviour and End Effects in water-wet porous media. Journal of Petroleum Technology.

Leverett, M. C. (1941). Capillary Behavior in Porous Solids. Society of Petroleum Engineers.

Lyons, W. (1996). Standard handbook of petroleum and natural gas engineering (Vol 2., Chapter 5). Houston, Texas: Gulf Publishing Company.

Maini, B. B., Ionescu, E., & Batycky, J. P. (1986). Miscible Displacement Of Residual Oil - Effect Of Wettability On Dispersion In Porous Media. Petroleum Society of Canada.

Mohanty, K. K. and Miller, A. E. (1991). "Factors Influencing Unsteady Relative Permeability of a Mixed-Wet Reservoir Rock. Society of Petroleum Engineers.

Mohanty, K. K. (1983). Multiphase Flow in Porous Media: III. Oil Mobilization, Transverse Dispersion, and Wettability. Society of Petroleum Engineers.

Morrow, N. R. and Mason, G. (2001). Recovery of oil by spontaneous imbibition. Current Opinion in Colloid & Interface Science, v. 6, no. 4, p. 321-337.

n-decane data-sheet (2018).
https://www.sigmaaldrich.com/catalog/product/sial/457116?lang=en&region=NO.

Osoba, J. S., Richardson, J. G., Kerver, J. K., Hafford, J. A., and Blair, P. M. (1951). Laboratory Measurements of Relative Permeability. Society of Petroleum Engineers.

Peksa, A.E, Wolf K-H AA, Zitha, P.L.J. (20015). Bentheimer sandstone revisited for experimental purposes. Marine and Petroleum Geology, v. 67, p. 701-719.

Qadeer, S., Dehghani, K., Ogbe, D.O., and Ostermann R-D., (1988). Correcting Oil/Water Relative Permeability Data for Capillary End Effect in Displacement Experiments. SPE California Regional Meeting, Long Beach, California. Society of Petroleum Engineers.

Quilon L and H data-sheet (2018).
https://www.sigmaaldrich.com/catalog/product/aldrich/420956?lang=en&region=NO

Richardson, J. G., Kerver, J. K., Hafford, J. A., and Osoba, J. S. (1952). Laboratory Determination of Relative Permeability. Society of Petroleum Engineers.

Salathiel, R. A. (1973). Oil Recovery by Surface Film Drainage In Mixed-Wettability Rocks. Society of Petroleum Engineers.

Skjaeveland, S. M., Siqveland, L. M., Kjosavik, A., Hammervold, W. L., & Virnovsky, G. A. (1998). Capillary Pressure Correlation for Mixed-Wet Reservoirs. SPE India Oil and Gas Conference and Exhibition, New Delhi, India. Society of Petroleum Engineers.

Tarek, A. (2001). Reservoir engineering handbook: Relative permeability concepts (2nd Ed., Chapter 3). Houston, Texas: Gulf Professional Publishing.

Tiffin, D. L. and W. F. Yellig (1983). "Effects of Mobile Water on Multiple-Contact Miscible Gas Displacements. Society of Petroleum Engineers.

Virnovsky, G. A., Skjaeveland, S. M., Surdal, J., & Ingsoy, P. (1995). Steady-State Relative Permeability Measurements Corrected for Capillary Effects. SPE Annual Technical Conference and Exhibition, Dallas, Texas. Society of Petroleum Engineers.

Virnovsky, G., Guo, Y., Skjæveland, S. (1995a). Relative permeability and capillary pressure concurrently determined from steady-state flow experiments. 8th European IOR-symposium in Vienna, Austria, May 15–17.

Virnovsky, G., Vatne, K., Skjæveland, S., Lohne, A. (1998). Implementation of multirate technique to measure relative permeabilities accounting for capillary effects. SPE Annual Technical Conference and Exhibition, 27–30 September, New Orleans, Louisiana.

Schlumberger (2006). Fundamentals of formation testing. Schlumberger Marketing Comunications. Sugar Land, Texas.

Sodium Chloride data-sheet (2018).
https://www.sigmaaldrich.com/catalog/product/aldrich/450006?lang=en&region=NO&gclid=EAIaIQobChMIkuOBm9ya3AIVkYKyCh0hOwwiEAAYASAAEgLZ9PD_BwE